UNIVERSITÀ DEGLI STUDI DI MILANO

Facoltà di Farmacia

Dipartimento di Scienze Farmaceutiche "P. Pratesi"

CORSO DI DOTTORATO DI RICERCA IN CHIMICA DEL FARMACO

XXIV CICLO

SETTORE CHIM/09 FARMACEUTICO TECNOLOGICO APPLICATIVO

TESI DI DOTTORATO DI RICERCA

SILK FIBROIN AS COMPONENT OF SCAFFOLDS FOR TISSUE ENGINEERING

Dr.ssa LAURA MAROTTA

Tutor: Prof.ssa Luisa Montanari

Coordinatore del dottorato: Prof. ERMANNO VALOTI

Anno Accademico 2010-2011

TABLE OF CONTENTS

General introduction

Tissue engineering / regenerative medicine is an emerging multidisciplinary field involving biology, medicine, and engineering that is likely to improve health and quality of life by restoring, maintaining, or enhancing tissue and organ function. The use of non-permanent scaffold materials that over time become completely replaced by natural extracellular matrix is central to the tissue engineering approach. The objective is to implant a scaffold that can persist in a robust state for sufficient time to allow the formation of new tissue, but which will ultimately degrade and become replaced by this tissue (1). Tissue engineering research includes different areas related to the various aspects involved in the regeneration of tissues and organs and among these one of the most important is the science of biomaterials that are used for the fabrication of scaffolds, supports for cell growth and proliferation. For functional tissue repair indeed, tissue engineering combines cells and bioactive factors in a defined microenvironment created scaffolds that are prepared from natural or synthetic polymers. The main demands on biomaterials for tissue engineering scaffolds are that they serve the bulk mechanical and structural requirements of the target tissue and enable molecular interactions with cells that promote tissue healing, including an interconnected network of pores for cell movement and mass transport of nutrients (1). Biomechanical aspects of design, including properties of native tissues, identification of minimum properties required of engineered tissues, mechanical signals regulating engineered tissues, and efficacy and safety of engineered tissues, should be then deeply considered in order to create a scaffold that can mimic the most closely the suitable microenvironment for cell proliferation and formation of a new functional tissue. Depending on the different features of the wide range of tissues considered, the scaffold structural requirements can vary considerably because the properties of the construct should resemble those at the implant site as closely as possible. For example, each

tissue presents its own set of demands: cortical bone is known for its high strength and toughness while constructs for soft tissues such as muscle or skin need to be flexible and elastic. Furthermore, most tissues exhibit anisotropy in their mechanical properties and a tubular scaffold for ligament replacement must be constituted of fibres regularly oriented along its longitudinal axis to confer it more tensile strength in the direction of force transmission. To replace soft tissue, instead, a high water content is important as well as the balance between strength and elasticity, strictly dependent from the crosslinking extent of the material. Considering this, great importance is assumed by the choice of the material for the scaffold preparation: the material should possess all the requirements needed for the cells to live and proliferate and to realize a scaffold that can respond to the requirements of the specific tissue to substitute. The scaffold material should be able to create a suitable architecture in order to fit the shape and dimensions of individual defect sites and should be versatile in order to confer to the scaffolds properties approximating those of the target tissue. The study of novel biomaterials is particularly significant because of the possibility of designing them for specific functional exigencies. In particular, the scaffold material should contribute with its structure to control and direct the organization and differentiation of cells in the process of forming functional tissue by providing both physical and chemical cues. Great importance can be assumed by a material that can be used for a wide range of applications, possessing characteristics that can be modulated to different demands and achieving widespread medical utility. In light of the considerations that we have shown up to this point, silk can be identified as a valid choice for the development of scaffold to be used in the field of tissue engineering.

Silks are generally defined as protein polymers that are spun into fibres by some lepidoptera larvae, such as silkworms, spiders, scorpions, mites and flies. The

most extensively characterized silk is from the domesticated silkworm Bombyx mori. B. mori silk fibres are mainly composed by two proteins, fibroin and sericin. Fibroin constitutes the core filament of silk, whilst sericin is a glue-like protein that holds two fibroin fibers together to form the composite fibres of the cocoon case to protect the growing worm.

B. mori silk has been used as biomedical sutures for centuries due to its mechanical properties and relative environmental stability. In literature, it was reported that virgin silk suture (containing sericin) induces hypersensitivity in patients, causing a Type I allergic reaction. As a consequence, over the last decades the use of silk in medical devices has declined since the arrival of commonly used absorbable and non-degradable synthetic sutures. After recognizing of sericin as the antigenic agent of silk, in the recent years the interest in the use of fibroin as biopolymer is growing (2).

Fibroin is constituted of highly organized beta-sheet crystal regions and semi-crystalline regions responsible for silk's elasticity compared to fibres of similar tensile integrity; it's the silk hydrophobic structural protein, which consists of a heavy chain (~390 kDa) and a light chain (~25 kDa). Silk fibroin's heavy chain is composed of large hydrophobic blocks, much smaller hydrophilic blocks, and two large hydrophilic blocks at the chain ends at the N and C termini (3). Silk fibroin's primary structure is dominated by the amino acids glycine, alanine, serine, valine and tyrosine with characteristic repetitive sequences of GAGAGS, GAGAGY and GAGAGVGY. These structural elements (large hydrophobic domains consisting of short side chain amino acids) permits tight packing of stacked sheets of hydrogen-bonded chains, forming the characteristic antiparallel β-sheet secondary structure that gives silk fibroin its strength and resilience (4).

Due to its peculiarities, silk fibroin is a suitable biomaterial in tissue engineering when mechanically robust and long-term degradable materials are needed, because it possesses unique properties that meet all the requirements for implantable applications. Silk fibroin shows excellent biocompatibility (5) and it degrades to non-toxic products *in vivo* and the degradation time course of silk implants can be controlled from weeks to years via regulation of sheet content (crystallinity) during processing (6). Furthermore, silk fibroin can be entirely aqueously processed using mild, ambient manufacturing conditions in order not to denature incorporated therapeutics. Fibroin is known to possess an aminoacidic sequence that is suitable for cellular adhesion, therefore it perfectly responds to the need of bearing coded complex information keeping the complexity to a minimum. Silk fibroin has been processed into a variety of useful material formats including porous tissue scaffolds for drug sustained release that structurally mimic the extracellular matrix. In addition, the properties of silk fibroin biomaterials can be tightly controlled during the fabrication process (7).

Regenerated fibroin is usually prepared by removing sericin and dissolving the two fibroin fibres by using aqueous solution containing high concentration of lithium or calcium salts. Then the obtained solution is dialyzed and the scaffolds are formed by causing the coagulation of the regenerated fibroin.

Fibroin scaffolds are proposed either to stimulate in vitro the cell growth (2D scaffolds) or to regenerate ligaments, cartilage and repair bone defects (3D scaffolds) (8). The 2D scaffolds are mainly prepared by simply casting the regenerated fibroin solutions at a constant temperature of about 60° C (9). 3D

scaffolds can be obtained by few methods, like particulate leaching, phase separation or electrospinning, but in this case freeze-drying method was selected because rather simple and able to create porous structures in a one step process, without the addition of any salts or other porogenous substances. The scaffold mechanical properties can be controlled by the coagulation method and the final curing that can modify the ratio between the beta-sheets (crystalline) and alpha-coils (amorphous) regions (10). The properties of fibroin scaffolds dependent from the crystalline fibroin amount are usually engineered by treating the scaffold with organic solvents after the preparation process. Nevertheless, the use of this kind of final curing can compromise the efficacy of loaded biologics and it's connected to problems related to the solvents disposal. To overcome such problems, new strategies were proposed to induce the fibroin conformational change to the crystalline β-sheet form. A possibility is represented by a sterilization treatment realized with the steam under pressure method, since it's known from literature (11) that heat and humidity can promote the fibroin conversion towards the stable β-sheet conformation. Another approach regards blending fibroin in solution with other polymers before the scaffold realization. Fibroin is blended mainly with chitosans, collagen, PEO and PVA. Composites made of fibroin and other biomaterials have been studied, but their application is generally limited to sore dressing or, more in general, wound dressing.

The eligibility of regenerated fibroin in tissue engineering is then well established, nevertheless few information are available on the mutual influence

of formulation and production conditions on the architecture and mechanical properties of fibroin scaffold. Regarding the formulation influence, the research was therefore focused on the impact of blending of regenerated fibroin with a suitable hydrophilic polymer, namely PEG with a molecular weight between 600 and 4000, on the 2D and 3D scaffold physico chemical characteristics. The evaluation of the effect of different fibroin concentration in the regenerated fibroin solution and of the addition of small amounts of organic solvents to the fibroin solution before the drying process was also considered. Regarding the 2D scaffold preparation, casting and spray-drying methods were considered. Regarding the 3D scaffold preparation, aim of this work was to go deeper inside the study of the freeze-drying process conditions that up to now was not systematically investigated. The experimental work was organized in the different steps and the obtained results were presented in three papers describing the stages of the experimental work:

- An investigation into silk fibroin conformation in composite materials intended for drug delivery
- Tuning the architecture of 3D scaffold made of fibroin by freeze-drying
- 3D fibroin composite scaffold for tissue engineering: preparation by freeze-drying, sterilization and characterization.

The first one was accepted for publication, the other 2 are going to be submitted.

References

(1) Place E. S. et al, *Chemical Society reviews*, 2009, *38*(4), 1139-51

(2) Altman G. et al, Silk-based biomaterials, *Science, 2002*

(3) McGrath K. & Kaplan D.L., *Protein-based materials*, 1997

(4) Meinel L. et al, *Biomaterials*, 2005, *26*(2), 147-55

(5) Vepari C. & Kaplan D.L., *Engineering*, 2009,*32*, 991-1007

(6) Wang Y. et al, *Biomaterials*, 2008, *29*(24-25), 3415-28

(7) Pritchard E. M. & Kaplan D.L., *Expert opinion on drug delivery*, 2011, *8*(6), 797-811

(8) Kirker-Head C. et al, *Bone*, 2007, *41*(2), 247-55

(9) Hines D.J. & Kaplan D.L., Biomacromolecules, 2011, 12, 804-812

(10) Zhan J. et al, *Chinese Science Bulletin*, 2007, *52*(13), 1791-1795

(11) Lawrence B.D. et al, *Journal of Materials Science*, 2008, 43, 6967–6985

Chapter 1

An investigation into silk fibroin conformation in composite materials intended for drug delivery

1.1 INTRODUCTION

Silk fibroin, a naturally occurring protein spun by the silkworm Bombyx mori, is a promising biomaterial for the incorporation and delivery of a range of therapeutic agents due to its unique properties such as slow biodegradation, good mechanical properties, and favourable processability in combination with biocompatibility (1). Several drug delivery constructs with different morphologies such as films (2), microspheres (3), nanoparticles (4) and hydrogels (5), have been proposed to control the release of both small molecule drugs and proteins, such as enzymes and cell growth factors. Natural silkworm silk fibres form predominantly crystalline β-sheet structures leading to stability, long-time degradability and the unique mechanical resistance (6). However, in order to prepare drug delivery systems, it is necessary to dissolve silk fibres in a solvent capable of denaturing the fibroin by breaking the strong intermolecular hydrogen bonds (7). Once the silk protein is dissolved, it can be processed into a variety of different material morphologies by different processes. Afterwards, a final curing is often required to enrich regenerated silk fibroin (SF) in β-sheet structure and, thus, induce water insolubility. This particular structure of SF is generally controlled by stretching, compression, annealing and/or chemical treatment in order to tune-up mechanical and degradability properties of films (8). Additionally, the correlation between conformation of SF and drug release was also reported (2): the higher the

crystalline content of SF, the slower the release of the encapsulated proteins. The ability to regulate the structure and morphology of SF in an all-aqueous process and/or mild processing technologies renders this biomaterial an important candidate for drug delivery applications. Furthermore, the use of final curing should be minimized, or even circumvented in order to incorporate efficaciously sensitive biologics and reduce detrimental and/or toxic effects of residual solvents. To overcome these drawbacks, the blending of SF with natural or synthetic polymers (9) has also been considered since SF and the auxiliary material might mutually aggregate to form a new ordered structure, which may guarantee the required mechanical strength as well as water insolubility avoiding post-treatment. In particular, the mechanical properties of regenerated SF have been improved by mixing with poly (ethylene glycol) 400 (PEG 400) (10). The purpose of the present study is to expand the understanding of the effects of blending SF with other hydrosoluble polymers and drying conditions on the conformation of the dried SF. With this aim, composite materials based on SF and poloxamer 35 (PEO), poly (vinyl pyrrolidone) (PVP) or a homologue series of poly (ethylene glycol) (PEG) were prepared by spray-drying or casting methods. These evaporation conditions were selected in order to evaluate also the effect of the evaporation rate other than the composition of the composite material on the SF conformation.

1.2 MATERIALS AND METHODS

1.2.1 Materials

Lutrol® F 68 (Poloxamer 188, PEO, Mw = 8600 Da) and Kollidon® K30 (poly (vinyl pyrrolidone), PVP) were kindly gifted by BASF (Germany). Poly(ethylene glycol) 4000 (PEG4000; hydroxyl value = 26–32 mg KOH/g; Mw = 3600–4400 Da) and poly(ethylene glycol) 600 (PEG600; hydroxyl value = 170–208 mg KOH/g; Mw = 540–660 Da) were provided by Polichimica (Italy), poly(ethylene glycol) 1000 (PEG1000; hydroxyl value = 102–125 mg KOH/g; Mw = 900–1100 Da) and poly (ethylene glycol) 1500 (PEG1500; hydroxyl value = 68–83 mg KOH/g; Mw = 1350–1650 Da) were purchased from Sigma–Aldrich (Italy).

1.2.2 Preparation of regenerated fibroin solution

Regenerated fibroin solution (SF) was obtained by degumming raw B. mori silk and dissolving the degummed silk fibres (about 7.2 g) in 100 mL $CaCl_2$ hydroalcoholic solution ($CaCl_2$/H2O/EtOH, mole ratio 1:8:2) at 70 ◦C for 2 h and shaken at 200 rpm in a thermostated bath. The regenerated fibroin was dialyzed in a cellulose tube (MWCO 12,000 Da, Sigma–Aldrich, Italy) against distilled water for 3 days at room temperature to remove salts and ethanol. The final solution was filtered with a metallic strainer and, then,

centrifuged for 20 min at 5000 rpm to eliminate the precipitated fibroin. The final fibroin solution concentration was about 3% (w/w), determined by weighting the remaining solid after drying.

1.2.3 Drying process

Spray drying: The feed was obtained by blending the fibroin solution and the selected polymer, namely PEO, PVP, PEG1000 and PEG4000, in the 95/5% (w/w) ratio. The feed was sprayed through a standard nozzle with inner diameter of 0.6 mm (Lab-Plant model SD04, UK). Process parameters: inlet temperature 130 ◦C; outlet temperature 85 ◦C; feed flow rate 11 mL/min. The pure regenerated SF was spray dried according to the same procedure. Casting method: The selected polymer, namely PEO, PVP and PEG1000, were added to 3% (w/w) SF solution in the ratio 5/95% (w/w) and gently stirred at room temperature to homogeneously disperse. Afterwards, the solution was casted on the bottom of a polystyrene Petri dish and dried in an oven thermostated at 60 ◦C until constant weight. The cast material made only by the regenerated SF was also prepared according to the same protocol. The effects of PEG molecular weight and SF/PEG ratio on the molecular conformation of SF were investigated. Films at PEG/SF ratio ranging from 99/1 to 60/40% (w/w) were prepared by using PEG600, PEG1000, PEG1500 and PEG4000.

1.2.4. Scanning electron microscopy

The surface morphology and shape of the spray-drying materials were analyzed by SEM (JSM-T 800-JEOL, I). The samples were sputtered with an Au/Pd coating in an argon atmosphere.

1.2.5. Thermal analysis

DSC data were recorded by using a DSC 2010 TA (TA Instruments, USA). The samples were sealed in aluminum pans and heated in inert atmosphere (70 mL/min N2) at 20 K/min from 30 to 350 ◦C. The reference was an empty pan. The equipment was calibrated with an indium sample. All measurements were performed in duplicate. The residual water content in the SF and SF/polymer materials was determined by thermogravimetric analyses using a TGA 2050 thermogravimetrical analyzer (TA Instruments, USA). Samples of approximately 20 mg were heated in a platinum crucible at 5 K/min under a nitrogen atmosphere and the loss of weight was recorded.

1.2.6. Attenuated total reflection Fourier transform infrared spectroscopy (ATR-FTIR)

FTIR measurements were performed using a SpectrumTMOne spectrophotometer (PerkinElmer, USA), by placing the samples on a diamond crystal mounted in ATR cell (PerkinElmer, USA). The spectra recorded at 2 cm^{-1} resolution and 32 scans were collected over the wavenumber region 4000–650 cm^{-1}. The analyses were performed on raw polymers and on spray-dried and cast materials. To assess the homogeneity in composition, FTIR spectra were recorded at least in three different points of the cast materials. Fourier self-deconvolution (FSD) of the overlapping amide I band components (1585–1700 cm^{-1}) was made possible by using Peakfit 4.12 software (Galactic Industries Corporation, New Hampshire, USA). Spectra were baseline corrected, smoothed with a nine-point Savitsky–Golay function (11). The amide I bands were resolved by the second-order derivative with respect to the wavelength. Deconvolution was performed using Gaussian line shape with an amplitude threshold of 3%. A nonlinear least-square method was finally used to take the reconstituted curve as close as possible to the original deconvoluted spectra. The fitting results were further evaluated by examining the residual from the differences between the fitted curve and the original curve.

1.3 RESULTS AND DISCUSSION

1.3.1. Effect of drying condition

Depending on the processing conditions, regenerated SF can preferentially assume random coil and β-sheet conformation (12). ATR-FTIR spectroscopy with Fourier self-deconvolution and DSC analysis are useful tools to investigate and quantify both contributions to the molecular conformations of this protein. The main differences reside in the position of absorption bands of amide I, amide II and amide III reflecting the different ratio between intra- and inter-molecular hydrogen bonds. In agreement with literature data, the degummed SF presented the characteristic β-sheet conformation (13) and the absorption bands of amide I, amide II and amide III were centered at 1620 cm^{-1}, 1511 cm^{-1} and 1227 cm^{-1}, respectively (**Figure 1**). In the same spectrum, two shoulders on the amide I and amide III bands were detected at 1696 cm^{-1} and 1265 cm^{-1}, respectively. In the ATR-FTIR spectrum of the spray-dried SF, the amide bands (amide I: 1638 cm^{-1}; amide II: 1515 cm^{-1} and amide III: 1233 cm^{-1}) were recorded at higher wavelengths and the shoulders on the amide I and the amide III were not detectable (**Figure 1**).

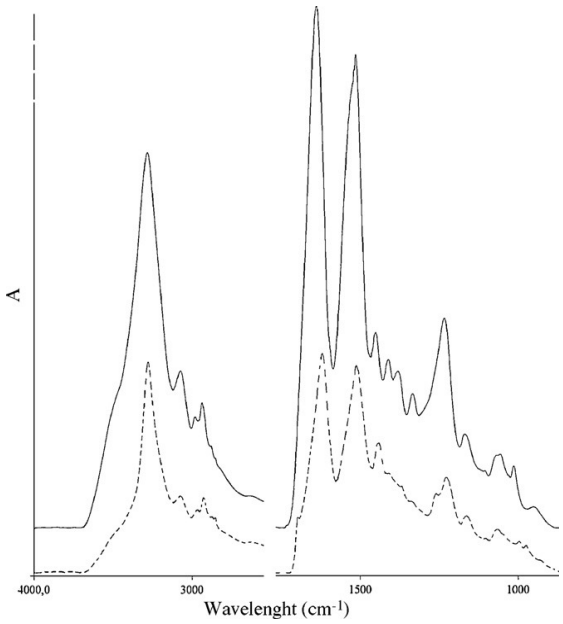

Figure 1. ATR-FTIR spectra of the degummed (dash line) and spray-dried SF (solid line).

These features were due to a prevalent random coil conformation (14). The spectrum of the cast SF was very close to that of the spray-dried SF, even if the bands assigned to amide I (1635 cm^{-1}), and amide III (1231 cm^{-1}) slightly shifted towards higher wavenumbers, suggesting the formation of a less disordered structure in the cast SF. DSC data confirmed the difference in spatial organization of the degummed SF, spray-dried and cast SF. The former pattern evidenced only the peak at about 300 ◦C attributed to thermal decomposition of the crystalline material after the endothermic event related to water evaporation at about 100 ◦C (**Figure 2**). The DSC profile of spray-dried SF showed the glass transition temperature at 179 ◦C, typical of the random coil conformation, followed by an exothermic peak at 218 ◦C (23 J/g) attributed to the transition from random coil to β-sheet

structure, and the thermal decomposition of the material at 299 ◦C (**Figure 2**).

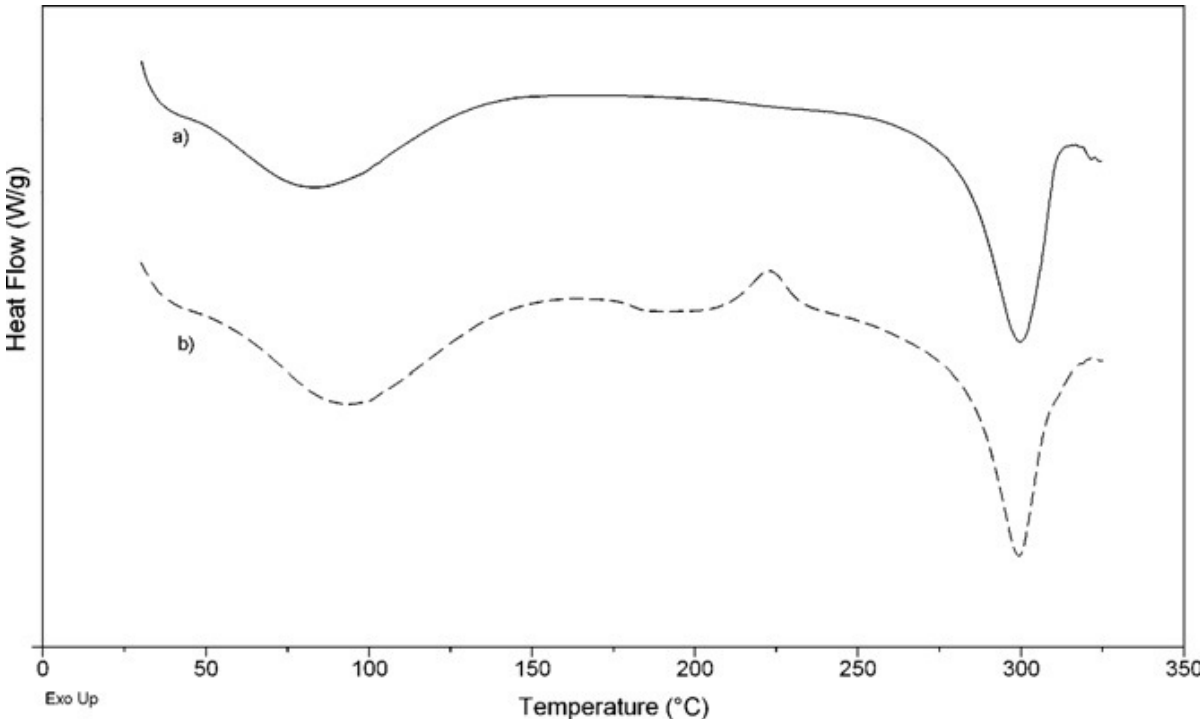

Figure 2. DSC data of the degummed (a, solid line) and spray-dried SF (b, dash line).

As expected, the thermal parameters of cast SF were superimposable to spray-dried SF (data not shown). The residual water content in the tested samples determined by a thermogravimetric method was about 7.5–10% (w/w). A deeper insight on the molecular conformation of SF dried according to the different procedures was carried out by Fourier self-deconvolution (FSD) of amide I region of the relative ATR-FTIR spectra. The deconvolution permitted to identify 11 peaks and the fitting revealed a good sound of correlation ($r^2 > 0.97$). **Figure 3a** and **b** reports Gaussian

curve fitting of the amide I region for the degummed and spray-dried SF, respectively. The amide I region bands were assigned to the different conformation of SF with reference to the literature (15). The band centered at about 1633 cm^{-1} was attributed to intramolecular β-sheet (B); the peak at 1699 cm^{-1} and the bands in the 1613–1625 cm^{-1} region are due to intermolecular β-sheets (B). In the region between 1667 and 1694 cm^{-1}, three or four peaks were found and assigned to the turn structure (T), which represents the less ordered crystalline structure (15). The contribution of the random coil (RC) conformation was represented by two peaks centred at about 1642 and 1651 cm^{-1}. The band assigned to the α-helices (A) was centred at 1659–1660 cm^{-1}. The absorption peaks related to the side chains or aggregated strands (SC) were detected in the 1595–1613 cm^{-1} region. The main difference in the deconvoluted amide I band of the degummed SF and spray dried product resides in the number of peaks assigned to the β-sheets. In particular, three intense bands assigned in the region from 1617 to 1637 cm^{-1} were found in the degummed SF and the weak β-sheet band at 1699 cm^{-1} was not detected in the spray-dried product. A further difference in the two deconvoluted spectra consists in the number of peaks attributed to the turns structure (**Figure 3a** and **b**). The pattern of the cast SF was ascribed to the spray dried product.

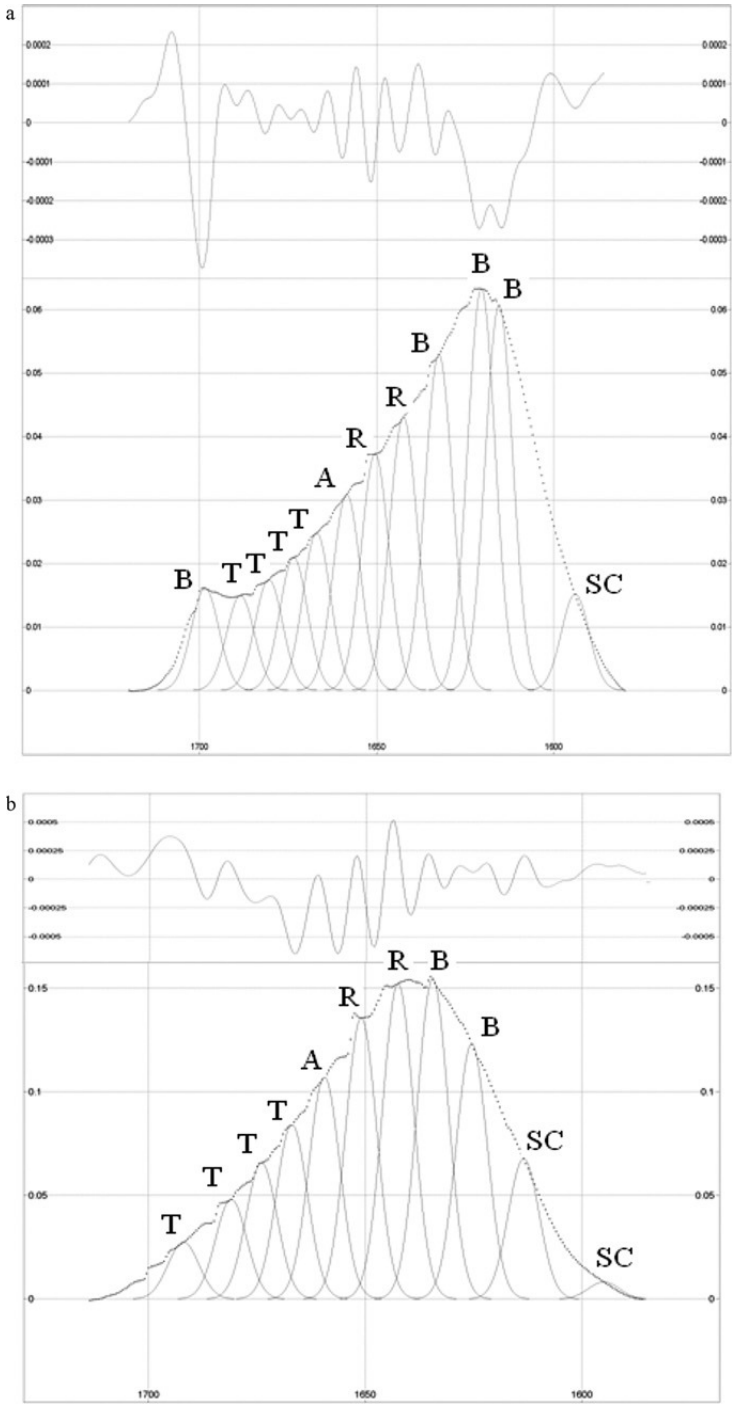

Figure 3. Absorbance spectra in the amide I region, deducted after Fourier transform self-deconvolution of (a) degummed and (b) spray-dried SF. The solid and dotted curves represent the original and the fitted spectra, respectively. The attributions of each deconvoluted band are marked as R (random coil), B (β-sheets), A (α-helices), T (turns), and SC (side chains). In the upper part of the graphs, the second derivative of the original spectrum was reported.

In order to better evidence the differences of SF spatial organization following different drying procedures, the relative amounts of the secondary structural elements were quantified by summing the area of peaks with the same attribution and the data were normalized with respect to the total amide I area (**Figure 4**). In both dried samples, the β-sheet fraction significantly decreased in parallel with the increase of the random coil/α-helices contribution with respect to the degummed SF. These events appear remarkable in the spray-dried sample, confirming that the faster the evaporation, the lower the ability of fibroin molecules to form an ordinate structure.

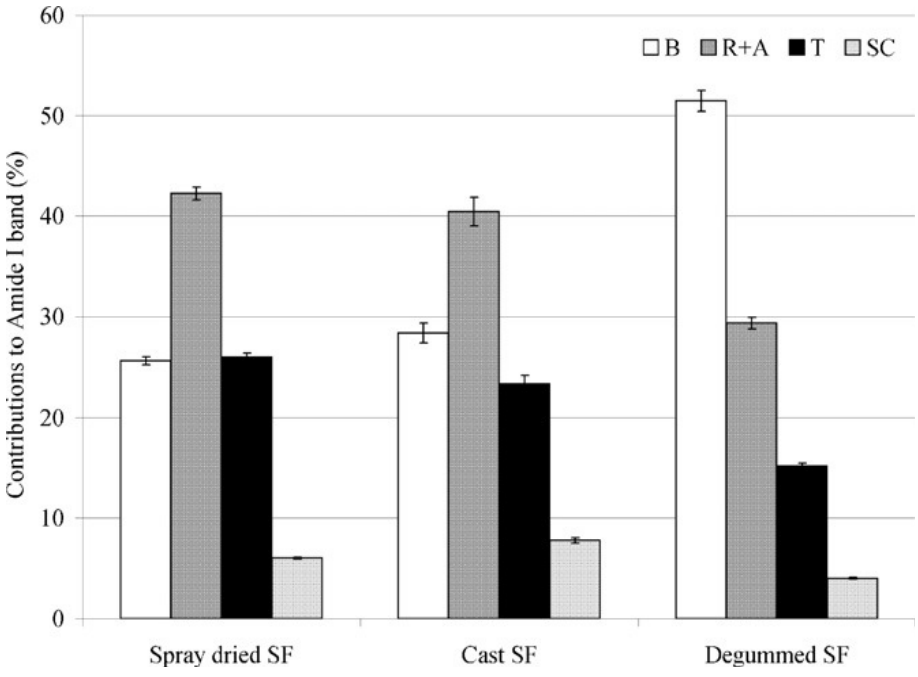

Figure 4. Contributions to the ATF-FTIR amide I band determined by Fourier transform self-deconvolution for regenerated SF as a function of the drying condition. Degummed SF was selected as control of crystallized sample. Each data point represents the percentage of the peak areas attributed to: β-sheets (B); random coils and α-helices (R + A); turns (T); side chains (SC). The coefficient of variation of these data lower was than 3.5 (n = 2).

1.3.2. Effect of the blending

The blending of SF to an auxiliary material is considered a suitable approach to induce the transition of SF from random coil to β-sheets (16). After mixing SF to PEO, PVP, PEG1000 and PEG4000 at the ratio of 5/95% (w/w), the solutions were dried by spray-drying or casting. The morphology of spray-dried blends appeared irregular (raisin-like structure) with a smooth surface. In the microphotographs no signs of inhomogeneity were evident independently of the nature of blended polymer (**Figure 5a–c**). The four materials obtained by casting procedure appeared smooth and transparent (data not shown).

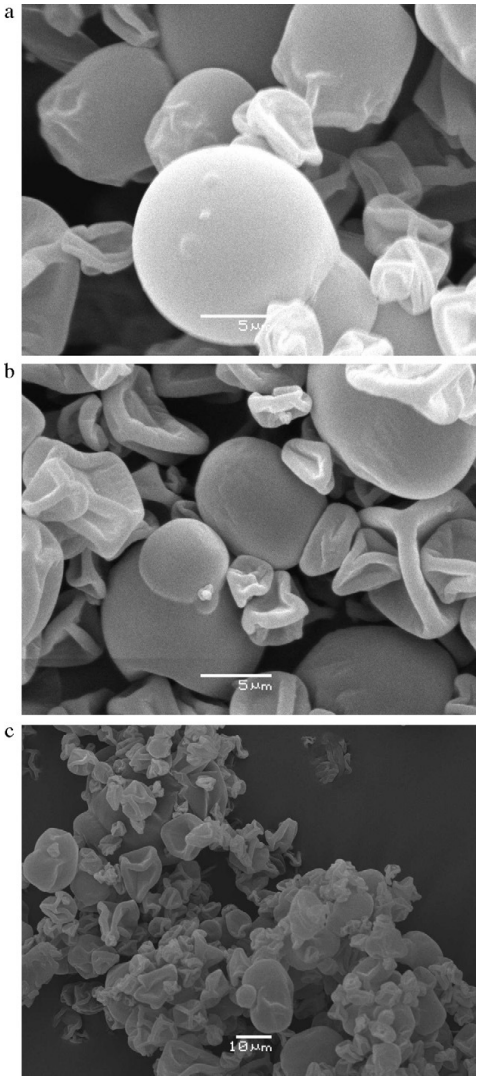

Figure 5. SEM microphotography of spray dried products made of (a) SF/PVP; (b) SF/PEO and (c) SF/PEG.

The spectra of spray-drying blends showed significant differences with respect to the degummed SF (**Figure 6**). Of particular interest is the amide III region since it allowed the discrimination among spray-dried blends. Indeed, the shoulders on amide I and amide III at about 1263 cm^{-1} attributed to the β-sheet conformation of SF (12) was detected only in presence of PEG4000. The analysis of deconvoluted amide I band confirmed these data. The amide I region of the spray-dried product made

of SF/PVP was not resolved because of an interference of the PVP stretching band detected at about 1645 cm^{-1}. The calculated contribution to β-sheets was in 24–26% for spray-dried SF/PVP, SF/PEO, and SF/PEG1000 products indicating that such materials were not effective to induce the transition towards an ordered structure since the calculated contribution to β-sheets were not statistically different from the spray-dried SF (one-way ANOVA, $p = 0.57$). In the case of spray-dried SF/PEG4000 the contribution to β-sheets resulted about 30% ($p < 0.01$). This partial conversion of SF to the crystalline structure after the rapid evaporation of the feed evidenced the key role played by the PEG average molecular weight.

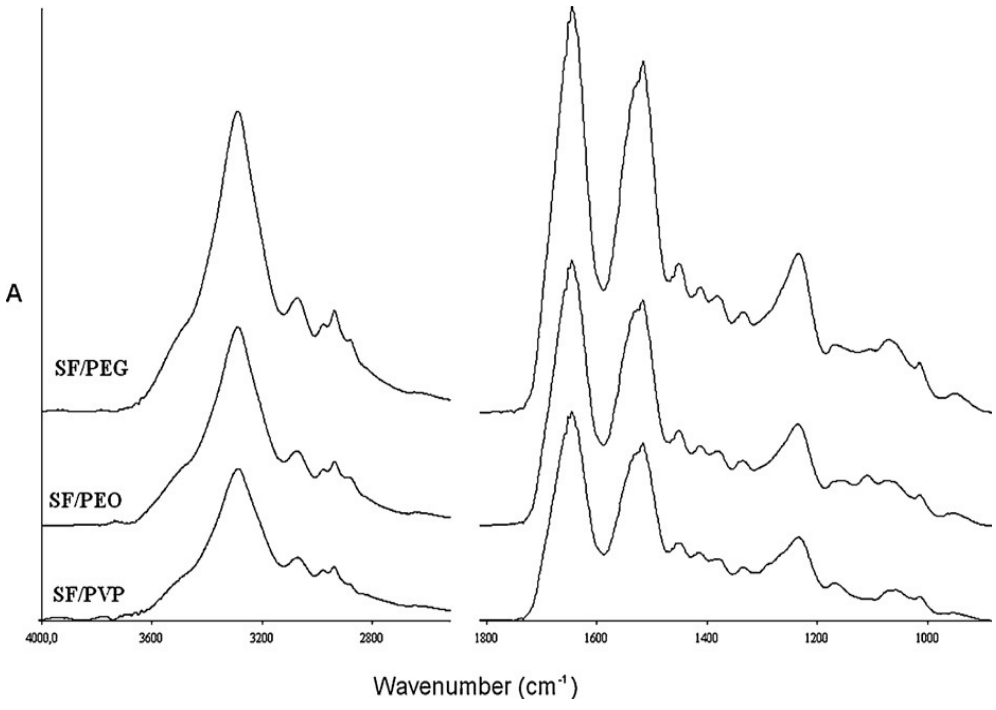

Figure 6. ATR-FTIR spectra of spray-drying products

Table 1. DSC data of spray-dried SF and blends at the ratio 95/5 (%, w/w).

	Tg (◦C)	Transition α→β			Degradation
		T_{onset} (◦C)	T_{max} (◦C)	ΔH (J/g)	T_{max} (◦C)
Spray-dried SF	181.0 ±1.1	211.6 ±0.3	220.7 ±0.7	23.08 ±1.	299.4±0.3
SF/PVP	182.2 ±0.9	213.8 ±0.7	225.2 ±0.4	29.2± 1.5	295.4±0.1
SF/PEO	181.7 ±1.4	209.1 ±0.4	221.2 ±0.3	32.3± 1.4	296.6±0.1
SF/PEG 1000	179.7 ±1.1	204.3 ±0.3	219.3 ±0.6	23.8± 1.4	296.7±0.2
SF/PEG 4000	181.0 ±1.3	201.1 ±0.2	219.5 ±0.3	16.2± 0.9	299.0±0.2

DSC results of spray-dried products indicated the typical thermal behaviors of the random coil structure. The glass transition temperature (Tg) was detected at about 180 ◦C independently of the blended polymers (**Table 1**). In presence of PVP, PEO and PEG1000, the transition from random coil to β-sheets occurred at temperature comparable to that measured for the spray-dried SF. The same transition in the SF/PEG4000 blend was recorded at higher temperatures with an increase in the enthalpy values, confirming the ability of PEG4000 in inducing the β-sheets conformation (**Table 1**). In the ATR-FTIR spectra of cast materials prepared by blending the

regenerated SF and the selected synthetic polymers, namely PEO, PVP, PEG 1000 and PEG4000 in the ratio 95/5% (w/w) SF molecules formed an ordered structure in the composite materials independently of the polymer blends since the main bands attributed to the amides stretching vibration overlapped with those of the degummed SF (**Figure 7**).

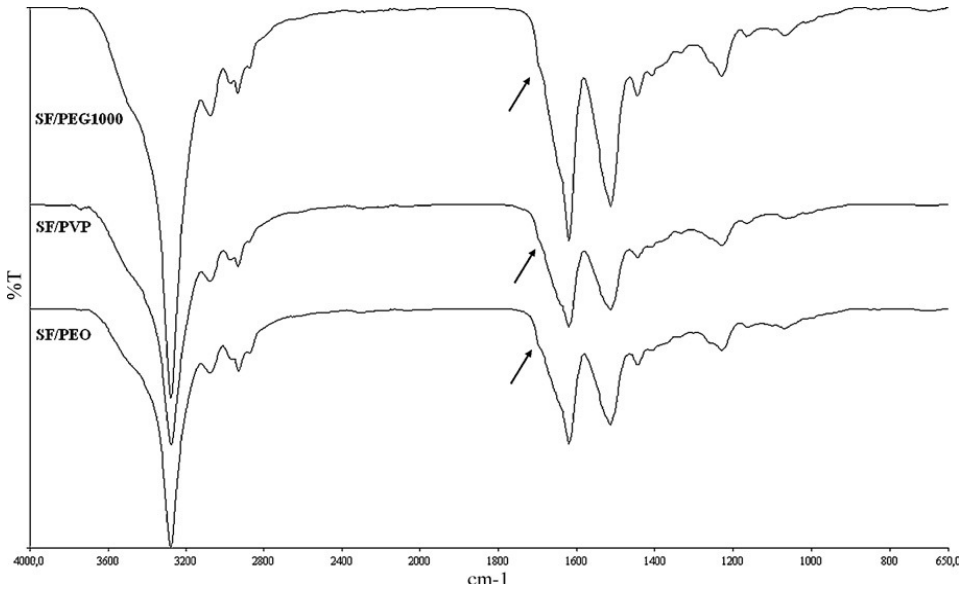

Figure 7. ATR-FTIR spectra of films prepared by blending the regenerated SF with PEO, PVP and PEG 1000 at 95/5% (w/w) ratio.

DSC data of the different SF/polymer blends obtained by casting revealed a single endothermic transition at about 297 ◦C attributed to thermal decomposition of SF (15), while the events due to the glass transition temperature at about 180 ◦C and the exothermic conversion from amorphous to crystalline at about 220 ◦C were not detected (**Figure 8**).

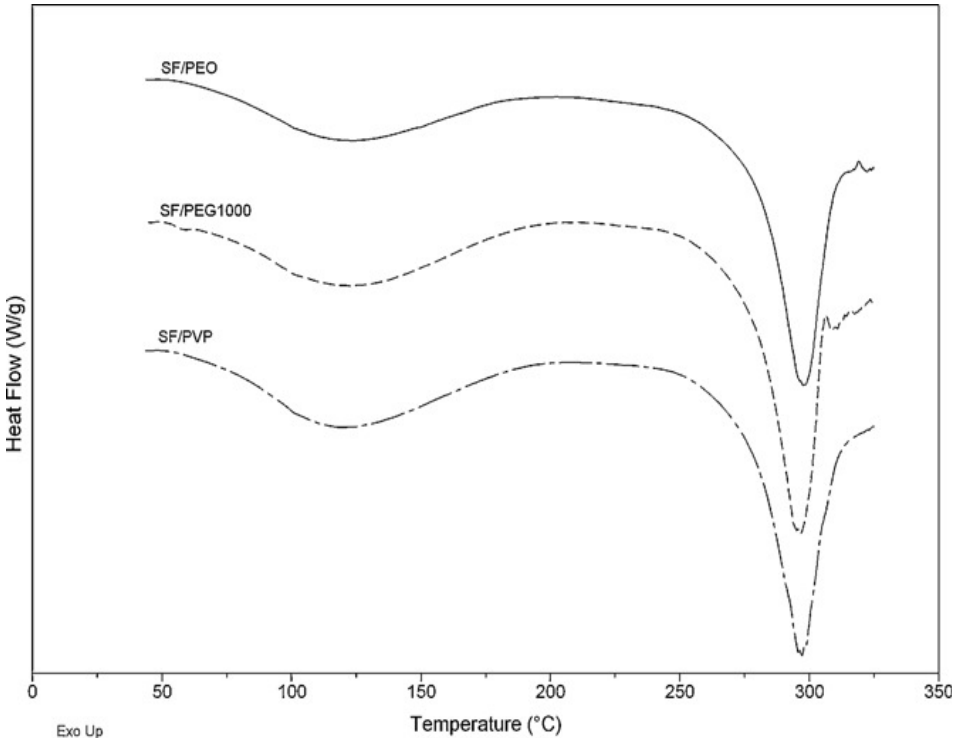

Figure 8. DSC data on films prepared by blending the regenerated SF with PEO (solid line), PVP (broken dash line) and PEG 1000 (dash line) at 95/5% (w/w) ratio.

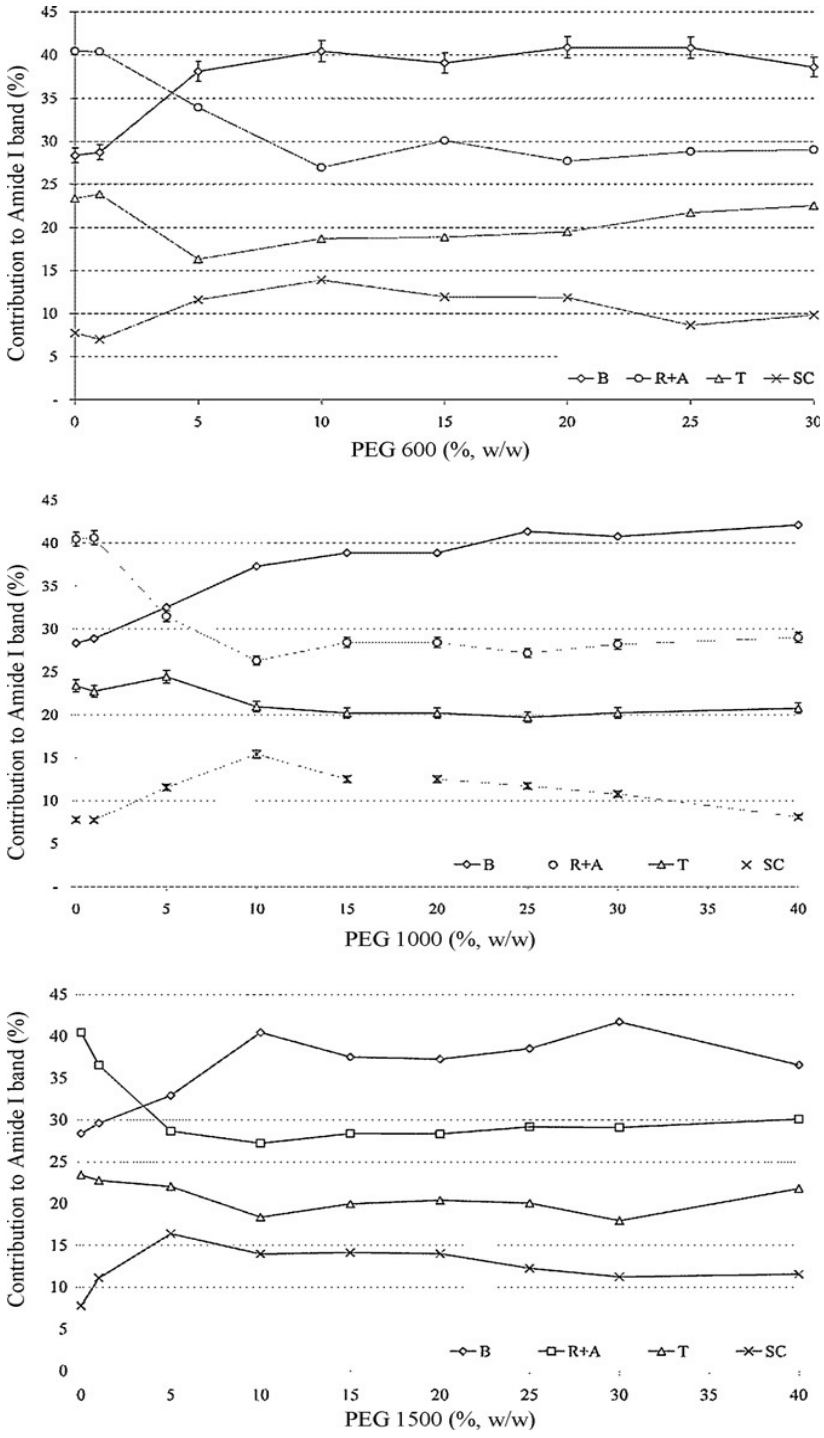

Figure 9. Contributions to the ATF-FTIR amide I band determined by Fourier transform self-deconvolution for regenerated SF in cast materials as a function of the SF/PEG ratio and PEG molecular weight. Each data point represents the percentage of the peak areas attributed to: β-sheets (B); random coils and α-helices (R + A); turns (T);side chains (SC). The coefficient of variation of these data lower was than 3.5 (n = 2).

On the basis of these findings, it can be assumed that the contemporary use of blending with the selected hydrophilic polymers at the ratio of 95/5%, w/w and the casting procedure promotes the transition of SF to the β-sheet conformation. Since PEG4000 was able to favour the β-sheet conformation of SF in the spray-dried material, it was considered worthily of investigation to study the effects of the PEG average molecular weights and PEG/SF ratios on the secondary structure of SF in cast materials. Four series were obtained by blending fibroin to PEG600, PEG1000, PEG1500 or PEG4000 and amide I of ATR-FTIR spectra were deconvoluted ($r2 > 0.96$). **Figure 9** shows the relative amounts of the secondary structural elements as function of SF/PEGs ratio. The contributions in presence of PEG4000 were not quantitatively reported because no reproducible data were obtained after casting the SF/PEG4000 blends at ratios higher than 95/5% (w/w). Indeed, the spectra recorded in different points of the cast materials did not overlap and the intensity of signals due to PEG4000 became more or less evident. The lack of miscibility in SF/PEG4000 cast material was also easily detected upon visual inspection: the material, generally homogeneous and transparent, became opaque and in some spots peeling features were evident (**Figure 10**).

Figure 10. Photography of a section of SF/PEG4000 film at the ratio 90/10% (w/w).

The molecular conformation of SF in cast materials prepared by using SF/PEG600 and SF/PEG1000 at the ratio 99/1%, w/w, was superimposable to the materials prepared by using the SF alone in terms of the relative amount of the secondary structural elements (**Figure 9**). At the same ratio, PEG1500 or PEG4000 (B = 31.6%,317 R+A=33.2%, T = 21.9%, SC = 13.3%) caused a slight increase of fractions of the β-sheets as well as side chains. The higher the amount of blended PEG in the cast materials, the higher the contribution of the β-sheet fraction to the total amide I band area. Increasing of the PEG amount in the blends, the β- sheet fraction reached the constant value of about 40% removing differences in terms of molecular weight and ratio among series and reaching values of crystalline closer to that of the degummed fibroin (~50%). These finding were also in

agreement with the DSC data. Indeed, when PEG600 was added to SF, the exothermic event recorded at about 206 ◦C was associated to a marked decrease in peak area (14 J/g). In addition, the higher crystallinity of the cast materials containing PEG4000 made the glass transition of the residual amorphous region less visible and more difficult to detect.

1.4 CONCLUSIONS

The amino acid composition (in mol %) of B. mori silk showed the predominance of five amino acids: Gly (42.9%), Ala (30.0%), Ser (12.2%), Tyr (4.8%), and Val (2.5%) (17). The primary structure of B. mori silk fibroin may be approximately divided into four regions: (i) highly repetitive GAGAGS sequences constituting the crystalline region, (ii) relatively less repetitive GAGAGY and/or GAGAGVGY sequences comprising semicrystalline regions containing mainly hydrophobic moieties, (iii) sequences similar to (i) plus an extension by AAS, and (iv) amorphous regions containing negatively charged, polar, bulky hydrophobic, and aromatic residues (17). The conformation of regenerated fibroin macromolecules and the transformation of their secondary structure are due to the rearrangement of the H-bonds especially in the (ii) regions. Even if these preliminary results should be deepened, it may be supposed that the tested synthetic polymers characterized by hydrogen acceptor groups, are able to form H-bonds with the tyrosine residues of SF which are largely located in the repetitive hexameric (–GAGAGY–) and octameric (–GAGAGVGY–) units of the semicrystalline regions (17). This feature can favour the formation of an ordered structure of these regions during the evaporation process and, therefore, the transition from the typical conformation of regenerated SF, namely random coil, towards - sheets.

This interaction is probably influenced by the density and distribution of the H-bond acceptor groups in the polymer backbone. Indeed, while the tested polymers are able to induce the transition of the semicrystalline regions towards the stable conformation at slow evaporation rate, PEG 4000 was the only polymer able to promote a partial organization of SF in the stable form after spray drying. Considering the homologous series of PEGs, higher the average molecular weight, i.e. the number of ether group for mass unit, higher the fraction of sheets as confirmed by the ATR-FTIR data of PEG4000/SF and PEG1000/SF spray dried products. In conclusion, the approach to prepare SF/hydrophilic polymers composite materials at slow evaporation rate leads to water insoluble construct. These blends obtained by all-aqueous process technologies could be advantageously used to load drugs with instability issues in silk-based delivery systems avoiding final curing.

References

(1) Vepari C & Kaplan D.L., Prog. Polym. Sci., 2007, 32, 991–1007

(2) Hofman S. et al, J. Control. Release, 2006, 111, 219–227

(3) Wang X et al, J. Control. Release, 2007, 117, 360–370

(4) Kundu J., Int. J. Pharm., 2010, 388, 242–250

(5) Numata K. & Kaplan D.L., Adv. Drug Del. Rev., 2010, 62, 1497–1508

(6) Cao Y. et al, Int. J. Mol. Sci., 2009, 10, 1514–1524

(7) Kaplan D.L., Protein-based Materials, Birkhauser, Boston, 1997, pp. 103–131

(8) Minoura N. et al, Biomaterials, 2009, 11, 430–434

(9) Hardy J.G. et al, Prog. Pol. Sci., 2010, 35, 1093–1115

(10) Wang S. et al, Chin. J. Pol. Sci., 2003, 21, 87–91

(11) Savitzky A. et al, Anal. Chem., 36, 1628–1639

(12) Hino T. et al, J. Colloid Interface Sci., 2003, 266, 68–73

(13) Boudet-Audet M. et al, App. Spectrosc., 2008, 62, 956–962

(14) Taddei P., Biopolymers, 2005, 78, 249–258

(15) Hu X. et al, Macromolecules, 2006, 36, 6161–6170

(16) Sashina E.S. et al., Russ. J. Appl. Chem., 2006, 79, 869–876

(17) Zhou C. et al, Nucleic Acids Res., 2000, 28, 2413–2419

.

Chapter 2

Tuning up the architecture of fibroin 3D scaffold by freeze drying

2.1 INTRODUCTION

Silk proteins are produced by a variety of insects, spiders and silkworm cocoons. The silk fibroin (SF) from the cocoon of silkworm Bombyx mori, the most studied silkworm silk proteins, contain two major components, light

(~25 kDa) and heavy chain (~325 kDa) fibroins (1). SF comprises highly

organized β-sheet crystal regions and semi-crystalline regions responsible for silk's elasticity. These two fibroins are encased in a sericin coat, glue-like proteins, to form the composite fibers of the cocoon. The utility of the regenerated SF has been expanded to biomaterials for cell culture and tissue engineering due to the combination of mechanical strength to versatility in processing and biocompatibility. Moreover, multiple material formats are available with silks, including films, fibers, sponges, and hydrogels, to provide versatility in uses. In particular porous SF sponges have been proposed as three-dimensional scaffolds by mimicking the structure and morphological features of native extracellular matrix, which provides mechanical support and regulates cell adhesion, proliferation and differentiation. Indeed, it is established that scaffold architecture and fibers orientation can control some cellular shape which dictates their function and influence tissue growth (2).

For instance, it is well established that scaffold topography controls hepatocyte shape which dictates the function of hepatocytes which can be improved by their culture in three dimensional systems, since these conditions more closely resemble the normal tissue environment than two dimensional culture conditions (3).

A wide range of techniques like salt leaching, freeze-drying, protein bubbling, and gas foaming could be used on these synthetic polymers to fabricate scaffolds with desired porous morphologies. Afterwards, a final curing is required to manipulate the secondary structure (i.e. the ratio between the β-sheets and random-coil regions) and, therefore, control several properties of silk-based materials, such as mechanical properties, solubility, and biodegradability.

The present work reports the impact of processing variables on morphology and mechanical properties of three-dimensional scaffold produced by freeze drying. In particular, the goal of the present study was expand the understanding of process and formulation parameters in order to obtain gradient silk-based biomaterials. Gradient biomaterials are biomaterials with anisotropic properties, such as composition, structure, mechanics and biomolecular properties. Gradient biomaterials are recent additions to the biomedical field for successful engineering of soft-to-hard interface tissues ("*interfacial tissue engineering*") which is a complex process requiring a

combination of specialized biomaterials with spatially organized material composition, cell types and signalling molecules (4).

Since sterility of scaffolds is a key parameter to assure the cellular growth, the influence of sterilization of vapour steam on molecular conformation and mechanical properties was investigated.

2.2 MATERIALS AND METHODS

2.2.1 Materials

Cocoons of B. mori silkworm silk were kindly supplied by ISMAC-CNR (Biella, Italy). All solvents and reagents were of analytical grade, unless specified.

2.2.2 Preparation of regenerated B. mori silk fibroin solutions

Regenerated fibroin solutions (SF) were obtained by degumming raw B. mori silk and dissolving an appropriate amount of the degummed silk fibres in 100 mL $CaCl_2$ hydroalcoholic solution ($CaCl_2/H_2O$/EtOH, mole ratio 1:8:2) at 70 °C for 2 hours and shaken at 200 rpm in a thermostated bath. The regenerated fibroin was dialyzed in a cellulose tube (MWCO 12,000 Da, Sigma-Aldrich, Italy) against distilled water for 2 days at room temperature to eliminate salts and ethanol present in the solution. The final solution was filtered with a metallic strainer and, then, centrifuged for 20 min at 5000 rpm to eliminate the precipitated fibroin.

2.2.3 Scaffold fabrication by freeze-drying

Glass vials, filled with 3 mL SF solution or the mixtures with *tert*-butanol (tBuOH) or dimethyl sulfoxide (DMSO) (**Table 1**), were placed on a pre-cooled shelf at -20 °C inside the ice condenser chamber of an Alpha 1-4 LSC Christ (G). The following freezing methods were used: *cooling strategy A:* when the complete solidification was evident, samples were maintained at -20 °C for at least 8 hours; *cooling strategies B and C:* once SF solutions reached the temperature of ice nucleation, the samples were thawed at 0 °C for about 1 hour (*cooling strategy B) or 2 hours (cooling strategy C)*. Afterwards, the freezing step was carried out according to the "*cooling strategy A".* Once frozen, all samples were dried under the following condition: *main drying:* The shelf temperature was ramped from -20 °C to 25 °C in 5 hours; afterwards it was kept constant for 8 h. The chamber pressure was set at 2.380 mBar; *final drying*: the chamber pressure was set at 0.001 mBar. The shelf temperature was kept at 35 °C for 4 hours. The final fibroin solution concentration ranging 1-4, % (w/w), was determined on the basis of the dry weight of scaffolds. Upon completion of the drying, the scaffolds stoppered under vacuum and stored at room temperature until use.

Table 1. Composition of scaffolds fabricated by freeze-drying.

Formulation code	Composition		Cooling strategies
	SF [a] (%, w/w)	Solvents [b] (2%, w/w)	
SF 1A	1	-	A
SF 2A	2	-	A
SF 3A	3	-	A
SF 3B	3	-	B
SF 3C	3	-	C
SF 4A	4	-	A
SF 3OH	3	tBuOH	A
SF 3SO	3	DMSO	A

[a] concentrations of SF in solution were determined on the basis of dried mass.

[b] the amount of solvents were calculated on the basis of the SF concentration in solution.

2.2.4 Scaffold sterilization

SF scaffolds were sterilized by vapour steam in autoclave (Tuttnauer 2540ML, The Netherland) at 121 °C and 1.2 mBar over 15 minutes.

2.2.5 Morphology

The morphology of scaffolds before and after sterilization was analysed by SEM (JSM-T 800-JEOL, Italy). The specimens were sputtered with an Au/Pd coating in an argon atmosphere then they were analysed with a spot of 3.5, 10 kV acceleration voltages and a WD of 10.

The surface and cross-section morphologies of the scaffolds and pore distributions, sizes, and interconnectivity were observed by MicroTC by MicroTC (SkyScan 1072 SKYSCAN, Be) adopting the following experimental parameters: voltage: 90 kV; current: 54 µA; rotational angle: 0.45°; layers' thickness: 20 µm.

The open porosity (π) of SF scaffolds was calculated by a solvent displacement method (5). The scaffolds were submerged in a known volume (V_1) of hexane that is not a solvent for SF and a series of brief evacuation–repressurization cycles was conducted to force the liquid into the pores of the scaffold. After these cycles, the volume of the liquid and liquid-impregnated scaffold was determined (V_2). When the liquid-

impregnated scaffold was removed, the remaining liquid volume was measured (V_3). The open porosity is calculated according to equation 1:

$$\pi = (V_1-V_3)/(V_2-V_3) \qquad \text{eq.1}$$

2.2.6 Molecular conformation

X-ray diffraction spectra of scaffolds before and sterilization were collected by using a Rigaku DMAX powder diffractometer (Rigaku, J) with Cu-Kα radiation and a monochromator on the diffracted beam.

FTIR measurements were performed using a Spectrum^{TM}One spectrophotometer (Perkin-Elmer, USA), by placing the samples on a diamond crystal mounted in ATR cell (Perkin-Elmer, USA). The spectra recorded at 2 cm^{-1} resolution and 32 scans were collected over the wavenumber region 4000–650 cm^{-1}. The analyses were performed on raw polymers and scaffolds before and after sterilization. Fourier self-deconvolution (FSD) of the overlapping amide I band components (1585-1700 cm^{-1}) was made possible by using Peakfit 4.12 software (Galactic Industries Corporation, New Hampshire, USA). Spectra were baseline corrected, smoothed with a nine-point Savitsky−Golay function (6). The amide I bands were resolved by the second-order derivative with respect to the wavelength. Deconvolution was performed using Gaussian line shape with an amplitude threshold of 3%. A nonlinear least-square method

was finally used to take the reconstituted curve as close as possible to the original deconvoluted spectra. The fitting results were further evaluated by examining the residual from the differences between the fitted curve and the original curve.

2.2.7 Mechanical properties

SF scaffolds were incubated in pH 7.4 PBS and stirred in a horizontal shaker incubator (50 strokes/min) at 37±1 °C (Julabo SW22, Germany). At specified time points (i.e. 7, 14, 21 and 28 days), specimen were removed and gently wiped. The mechanical properties of scaffolds were measured by a software controlled dynamometer (AG/MC, Acquati, Italy) equipped with a stainless steel probe (diameter: 4 mm) connected to a 5 daN force cell. Three samples of each scaffold were tested. The scaffolds were compressed at a cross head speed of 3mm/min. Load and displacement force was noted.

2.3 RESULTS AND DISCUSSION

2.3.1 Influence of formulation on characteristics of SF scaffold

Preliminarily a study was carried out aiming to define the optimal freezing time in order to obtain scaffolds with a satisfactory porosity and stability upon sterilization. It was defined that a minimum of 8 hours at the temperature of -20 °C is required to avoid collapsing structures after treatment with water vapour (**Figure 1**).

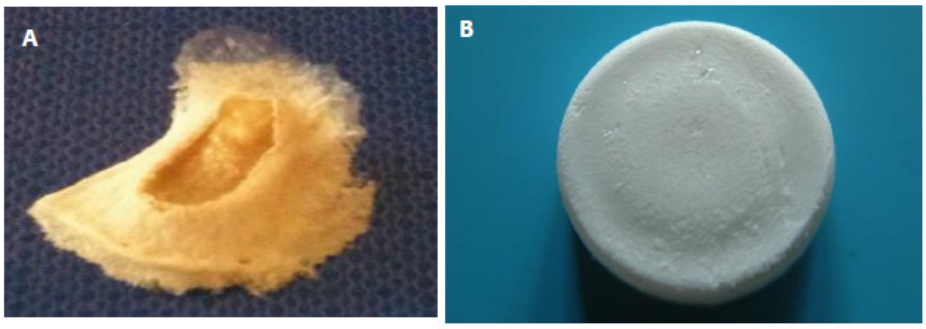

Figure 1: Photography of the sterile scaffold obtained after a (A) 4 hour and (B) 8 hour period of freezing.

Afterwards, the influence of formulation variables, namely the SF solution concentration and the presence of an organic solvent, on scaffolds prepared according to the *Cooling strategy A* was investigated. All matrices presented a homogeneous structure characterized by a sponge-like morphology. The lower the solution concentration, the higher the scaffold porosity (**Table 2**). After sterilization, both porosity and interconnection

were well-preserved independently of concentration of solutions and the presence of organic solvents, even if a slight reduction of the porosity of about 4-5% was determined (**Table 2**).

Table 2. Porosity of scaffolds fabricated by freeze-drying according the cooling strategies A before (BS) and after (AS) sterilization.

Formulation code	**Porosity (%)**	
	BS	**AS**
SF 1A	97%	92%
SF 2A	96%	90%
SF 3A	85%	80%
SF 4A	75%	70%
SF 3OH	85%	85%
SF 3SO	86%	82%

In order to evaluate the complex inner organization of scaffold structure which count not be determined by a porosity measurement , the samples were observed by SEM to verity the pore size as well as their interconnectivity. All scaffold presented a good interconnectivity with a pore dimension of about 50 μm (**Figure 2**).

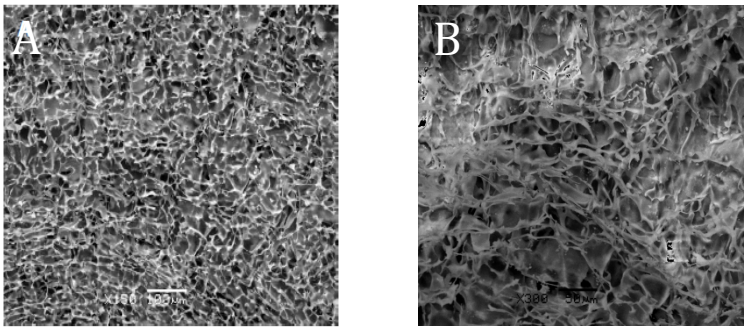

Figure 2: SEM photography of (A) inner and (B) surface of scaffold (SF concentration = 3%).

An insight on the molecular conformation of SF in scaffolds was carried out by FSD of amide I region of the relative ATR-FTIR spectra. As an example, **Figure 3** reports the deconvoluted amide I bands of the β-sheet conformation SF with reference to the literature (7).

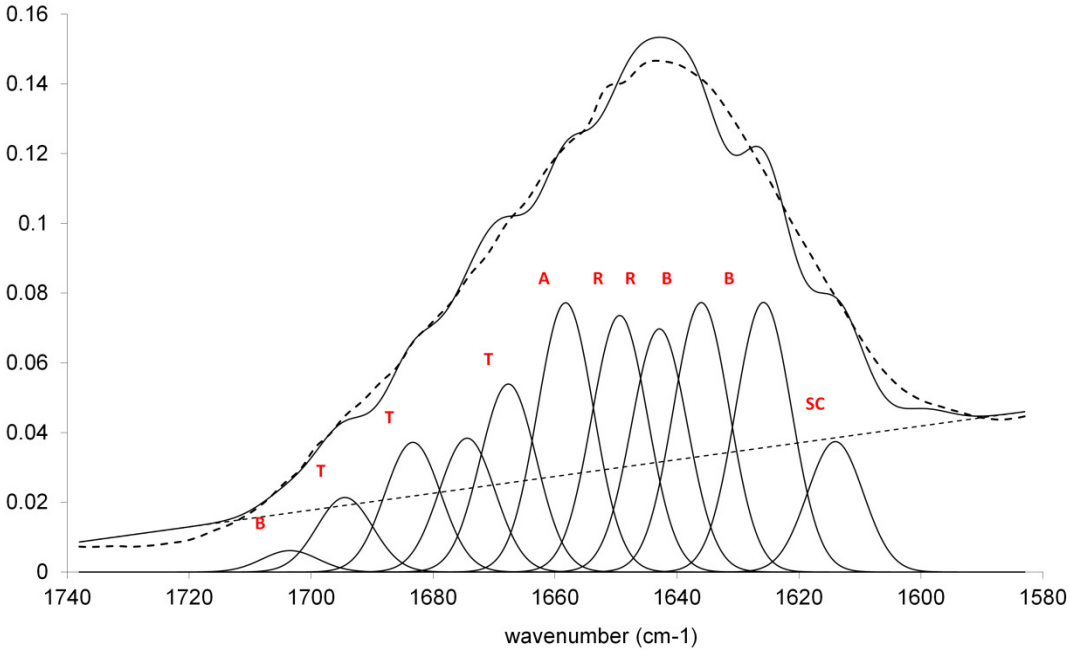

Figure 3: Deconvoluted amide I bands of the β-sheet conformation SF.

In order to better evidence the differences of SF spatial organization following different cooling procedures, the relative amounts of the secondary structural elements were quantified by summing the area of peaks with the same attribution, namely side chain (SC), β-sheet (B), β-turn (T), random coil and α-helix and (A+R) fractions, and the data were normalized with respect to the total amide I area. The contribution of peak areas attributed to different components was not influenced by the solution concentration and a prevalence of the random coil conformation was detected in all samples as represented in **Figure 4** for the formulation SF3A.

The addition of 1% of both DMSO and tBuOH to the formulation SF3A permitted to increase the β-sheet content in scaffold (**Figure 4**).

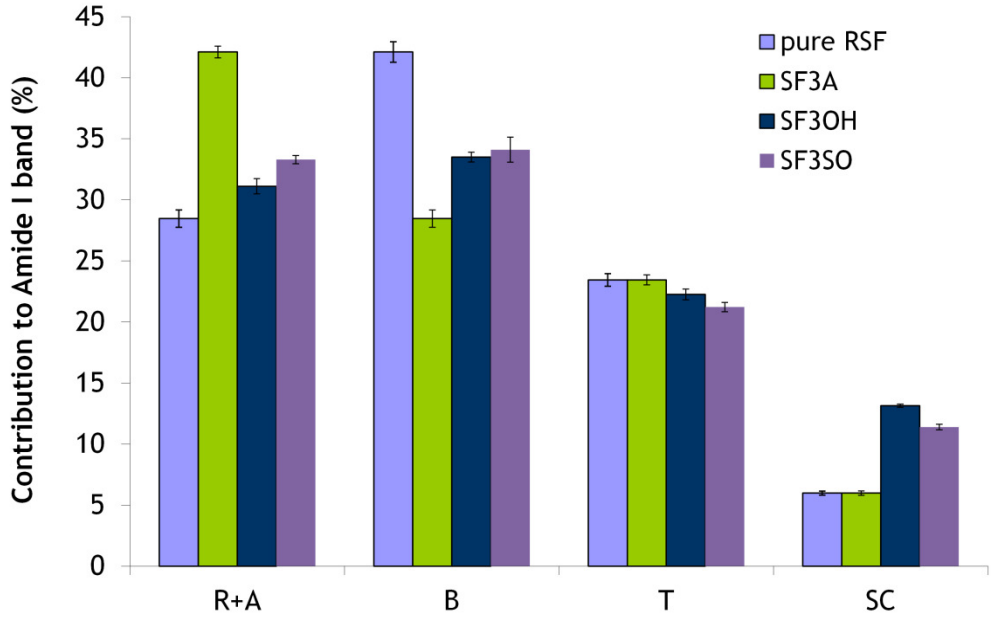

Figure 4: Contributions to the ATF-FTIR amide I band determined by Fourier transform self-deconvolution. Each data point represents the percentage of the peak areas attributed to: β-sheets (B); random coils and α-helices (R+A); turns (T); side chains (SC).

Steam sterilization induced a modification in the silk fibroin secondary structure content, causing an increase in the β-sheets content along with a decrease in α-helix/random coil content. Moreover, the differences in β-sheets content due to differences in formulation were annealed. As an example in **Figure 5**, the contribution to the ATF-FTIR amide I band in scaffold obtained from a 2% SF solution is reported. Similar results have

also been observed in recent studies exploring the temperature and humidity effects on silk films (8, 9, 10).

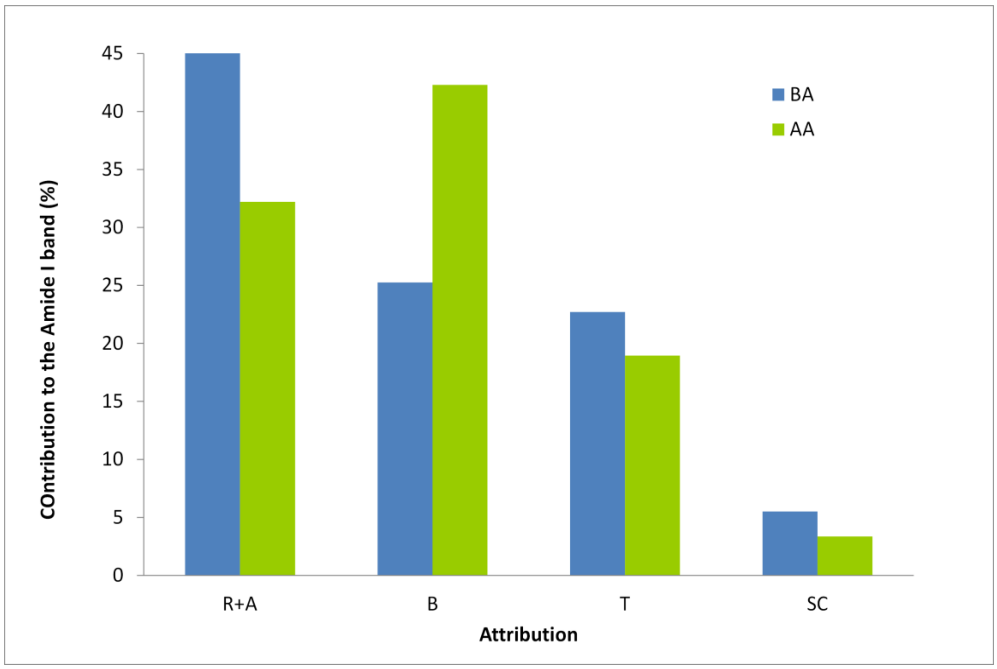

Figure 5: Contributions to the ATF-FTIR amide I band determined by Fourier transform self-deconvolution of scaffold SF2A before (BA) an after (AA) sterilization. Each data point represents the percentage of the peak areas attributed to: β-sheets (B); random coils and α-helices (R+A); turns (T); side chains (SC).

Structural changes in the SF scaffold before and after sterilization were also evaluated by X-ray diffraction. **Figure 6** shows XRD spectra of SF scaffolds before and after sterilization along with that of a pure silk fabric. After treatment in autoclave, peaks at 2Θ = 20-21° and 24-25° appeared in the XRD spectra compared with that of the noncrystalline structure before sterilization. The former is attributable to the silk II crystalline structure of

SF (11) of fibroin which is shown in the silk fabric XRD spectrum. This result indicates that the silk II crystalline structure occurred only after sterilization, but a qualitative comparison of the peak evidenced that the amount of the crystalline structure is smaller than that in the silk fabric. Peak at 24-25° was attributed to the silk I structure. Therefore, the XRD spectra indicate that both molecular conformations coexist in the SF scaffold. No remarkable differences were noticed in the XRD spectra of the SF scaffolds prepared by solutions at different concentrations as well as in presences of organic solvents (data not shown).

As far as the mechanical properties of the incubated scaffold are concerned, it can be noted that, as expected the resistance to compression increase decreasing the scaffold porosity (**Table 3**): The addition of the t-BuOH determine a dramatically reduction of the mechanical resistance of the scaffold which resulted unquantifiable (**Table 3**).

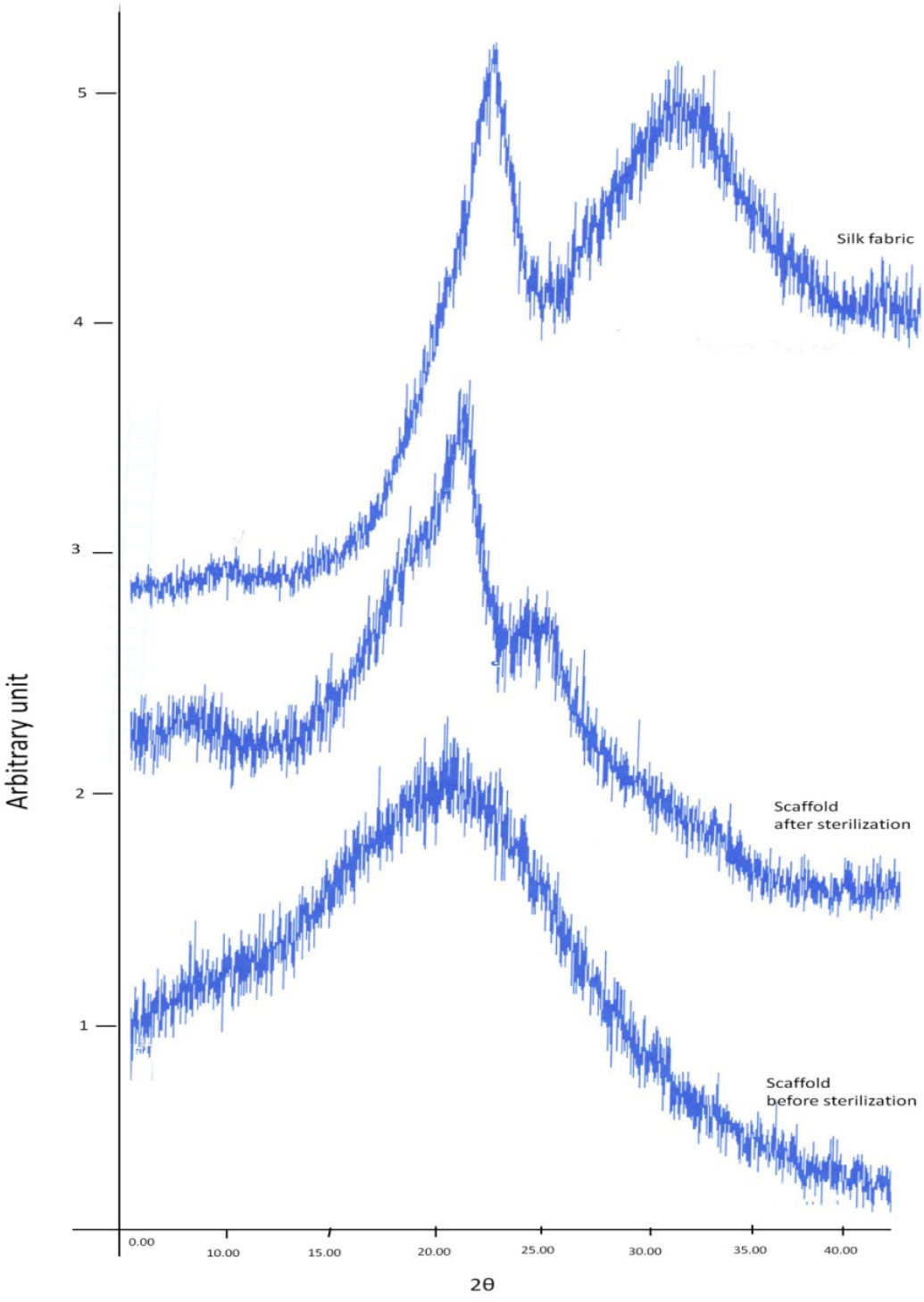

Figure 6: XRD spectra of SF scaffolds before and after sterilization along with that of a pure silk fabric

Table 3. Mechanical resistance test of different formulations of fibroin scaffolds

Formulation code	Mechanical resistance (N)			Elastic return (N)		
	0	7 d	14 d	0	7 d	14 d
SF 1A	0.03 ± 0.01	0.06 ± 0.03	0.02 ± 0.01	0.05 ± 0.04	0.05 ± 0.03	0.06 ± 0.02
SF 2A	0.17 ± 0.02	0.2 ± 0.06	0.15 ± 0.01	0.17 ± 0.02	0.18 ± 0.04	0.14 ± 03
SF 3A	0.22 ± 0.02	0.24 ± 0.06	0.21 ± 0.04	0.22 ± 0.04	0.23 ± 0.05	0.20 ± 0.02
SF 4A	0.52 ± 0.15	0.57 ± 0.06	0.53 ± 0.12	0.48 ± 0.12	0.54 ± 0.06	0.50 ± 0.11
SF 3SO	0.45 ± 0.18	0.51 ± 0.11	0.59 ± 0.11	0.43 ± 0.18	0.48 ± 0.10	0.56 ± 0.09
SF 3OH	-*	-	-	-*	-	-

* lower than 0.01 N.

On the bases of these results the concentration of 3% w/w fibroin was selected for the evaluation of process parameters because the scaffold SF3A was considered a suitable compromise between the scaffold porosity and its mechanical properties.

2.3.2 Influence of cooling strategy on the structural characteristics of SF scaffolD

Figure 7 reports the typical thermogram of a 3% SF solution frozen according to the different cooling strategies. In all cases, samples resulted supercooled at -8 °C prior to sharp increase to about 0°C. This temperature represents the point of completion of nucleation and the onset of solidification.

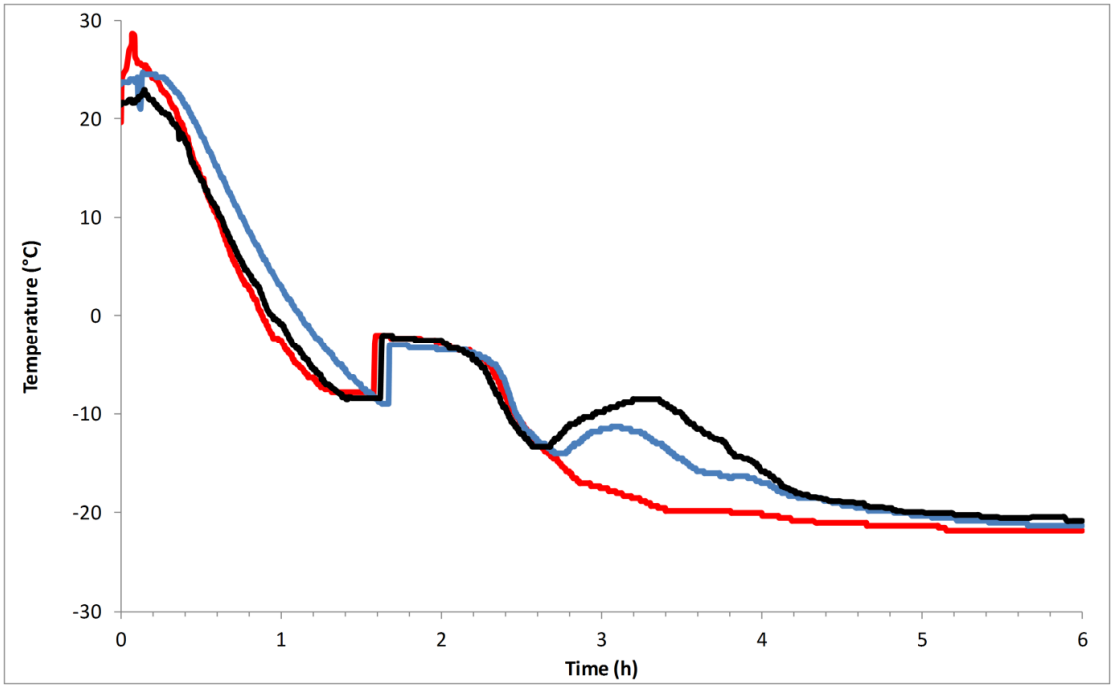

Figure 7: Thermograms of the different cooling strategies of 3% fibroin solution. Red line: cooling strategy A; blue line: cooling strategy B; black line: cooling strategy C

Afterwards, in *cooling strategy A* as solidification progressed to competition, the SF sample temperature gradually equilibrated with that of the shelf. Samples nucleated and froze via the global supercooling mechanism, namely the entire liquid volume achieves a similar level of supercooling and the secondary nucleation zone encompasses the entire liquid volume (12). As a consequence, the spherulitic morphology in the corresponding scaffold type A is probably due to the formation of spheroidal ice crystals concentrated the amorphous phase into a sponge-like matrix.

Figure 8 and **9** show SEM and microTC images of scaffold type B produced according to the *cooling strategy B*. Two layers at different morphologies were clearly distinguished: the upper part presents an oriented stacked leaf-like structure oriented toward the centre of the matrix (**Figure 9 a-c**) and the lower part results in a sponge-like matrix (**Figure 9 a-b**). It can be assumed that the SF solutions initially underwent to a complete freezing as occurred in samples underwent to the *cooling strategy A*. Afterwards, increasing the shelf temperature, the movement of chain segments in SF was activated, which made possible for water or small ice particles in an unstable phase to move towards the surface of large particles. This allows the ice crystals to rearrange and grow to a more stable state and the number of ice particles per volume decreased correspondingly. When the freezing conditions were stressed by introducing a longer thawing step in the *cooling strategy C,* the scaffolds presented a uniform morphology in

which the sponge-like matrix was completely substituted by the stacked leaf-life structure corresponding to lower layer in scaffold of **Figure 8**.

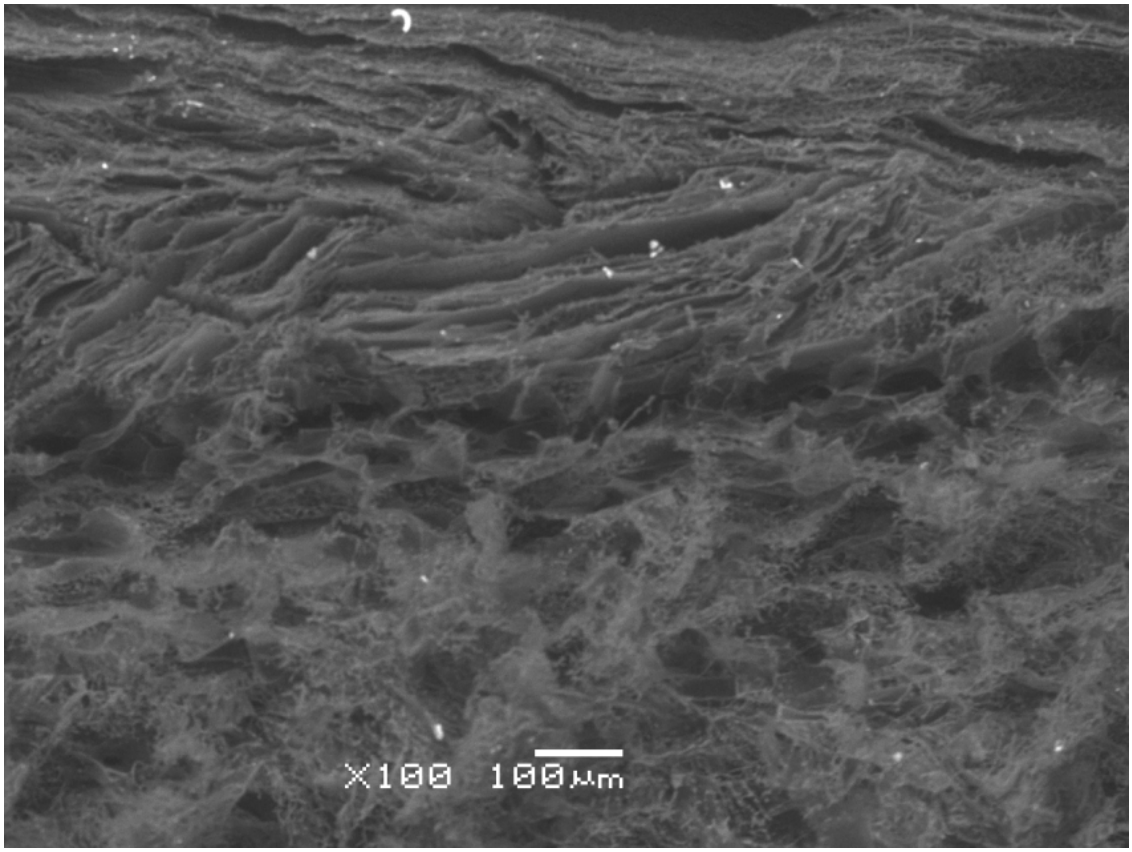

Figure 8: SEM of scaffolds frozen according to the cooling strategy B.

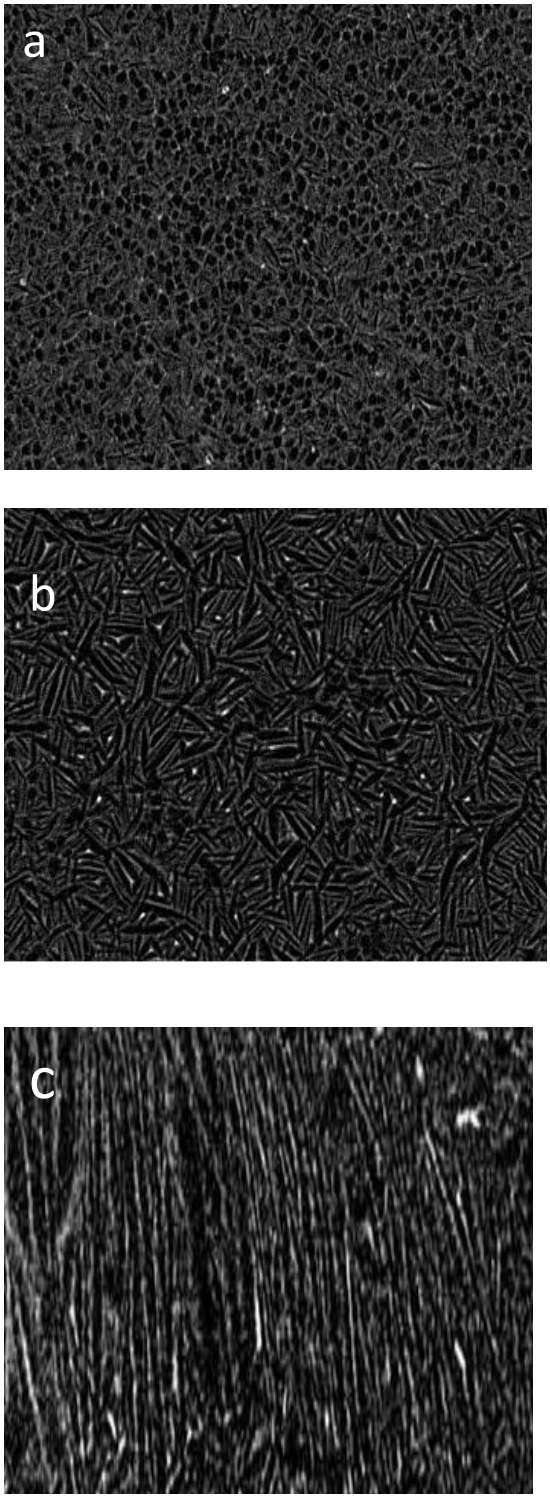

Figure 9: Micro-CT of scaffolds frozen according to the cooling strategy B: a) transversal section of the sponge-like layer b) transversal al section of the leaf -like layer c) horizontal section of the leaf-like layer

Differences in morphology determined differences in the porosity of scaffolds which increases from 85% to about 94% shifting from a sponge-like structure towards the leaf-like structure (**Table 4**).

Table 4. Porosity of scaffolds fabricated by freeze-drying according the different cooling strategies before (BS) and after (AS) sterilization.

Formulation code	**Porosity (%)**	
	BS	**AS**
SF 3A	85%	80%
SF 3B	87%	84%
SF 3C	94%	92%

When the material slurries froze according to the *cooling strategy A,* the corresponding scaffolds were mainly composed of amorphous silk I structures independently of the solution concentration. Upon the *cooling strategies B*, SF scaffolds presented a higher amount of β-sheet fraction in the lamellar-like structure with respect to the sponge-like portion (**Table 5**).

Table 5. Total contribution (%) to secondary structural elements of amide I band in sponge- and lamellar-like structures of scaffolds prepared according to the cooling strategy B before (BS) and after (AS) sterilization (SE < 1%).

	sponge-like		**lamellar-like**	
	BS	**AS**	**BS**	**AS**
Side chain	5.98	13.07	4.4	4.6
β-sheet	28.46	35.40	33.8	33.5
Random coil and α-helix	42.11	31.28	41.8	40.6
β-turn	23.45	20.26	19.8	21.5

The different spatial organization of the scaffold fibers obtained by the two cooling procedures lead to significant different mechanical properties as exemplified in **Figure 4**. The strongest resistance of the lamellar-like

structure of scaffolds was mainly attributed to the lamellae fibers oriented towards the z-axis.

2.4 CONCLUSIONS

In conclusion, the morphology of sterilized SF scaffold can be easily varied by modulating the freezing step during the lyophilisation process or adding small amounts of organic solvents. This data suggested that fibroin can be used for producing gradient scaffold by one step process.

REFERENCES

(1) Altman G.H. et al, *Biomaterials*, 2003, 24(3), 401–416

(2) Wendorff et al., *Polymer* , 2008, 49(26), 5603-5621

(3) Funats K. et al, *Organs*, 2001, 25, 194–200

(4) Azadeh S. et al, *Acta Biomaterialia*, 2011, 7, 1441–1451

(5) Karageorgiou V. et al, *Biomaterials*, 2005, 26(27), 5474-5491

(6) Savitzky A. et al, *Analytical Chemistry*, 1964, 36, 1628−1639

(7) Cilurzo F. et al, *International Journal of Pharmaceutics*, 2011, 414, 218-224

(8) Jin H.J. et al, 2004, *Biomacromolecules*, 5, 711

(9) Agarwal K. et al, *Journal of Applied Polymers Science*, 1997, 63(3), 401

(10) Hu X. et al, *Thermochemical Acta*, 2007, 461(1–2), 137

(11) Marsh R.E. et al, *Biochemical and Biophysical Acta*, 1955, 16, 1-34

(12) James A. et al, *Journal of Pharmaceutical Sciences*, 2001, 90(7), 860–871

Chapter 3

3D fibroin scaffold for tissue engineering: preparation by freeze drying, sterilization and characterization

3.1 INTRODUCTION

Within lesions repair and functional tissue regeneration, structures constituted by natural or synthetic polymers were developed. These kinds of structures are called “scaffold” and they combine in the same environment cells and growth factors. Scaffold can be projected in 2 (films or membranes) or 3 dimensions (sponges or fibers) with the aim of promote cells adhesion and stimulate their growth and differentiation. Scaffolds must be realized with materials that, beneath being highly biocompatible and biodegradable, are easily and allow obtaining highly porous constructs with a suitable mechanical resistance and dimensional stability (1). Due to its peculiarities, regenerated fibroin represents a suitable material to use in tissue engineering when mechanical stability and a slow scaffold degradation rate are required. Generally regenerated fibroin is obtained after silk sericin removal (degumming) and dissolution of the fibroin fibers and dialysis of the obtained solution. Scaffolds are obtained by coagulation of the regenerated fibroin solution. Scaffold mechanical properties can be modulated by varying the coagulation method and/or the final curing, since these processes can influence the ratio between the ordered zones (β-sheet) and the amorphous ones (random coil) (2). Fibroin scaffolds have been studied both for stimulating in vitro cell growth (2D scaffold) and for the restoration of structural and functional integrity of ligaments, cartilage and to promote the formation of new bone tissue (3D scaffold) (3). Fibroin degradation time and rate depend from the regenerated material form and from the implantation site.

Indeed, silk fibers used as suture threads are biodegradable in long terms (months, years) whilst regenerated materials like membranes or gels degrade in middle-short terms (weeks-days) (4). Normal production processes lead to the formation of structures with a protein organization prevalently in the random coil form and, consequently, with low water resistance and poor mechanical properties. On the contrary, it is necessary that fibroin used for the scaffold preparation assumed the β-sheet conformation, since matrices must present such mechanical properties to adequately support proliferating cells. Fibroin conversion to the crystalline form can be achieved by organic solvent treatment, like methanol, that is able to dehydrate protein chains (5). It was reported that the addition of polyethylene glycols with low molecular weight are able to induce the fibroin conversion in the stable β-sheet form (6) and consequently permit a remarkable increase in the mechanical properties of 2D scaffolds obtained by casting (7). 3D scaffolds made of fibroin are obtained from fibroin solution by means of a lyophilisation process or by salt leaching or gas foaming methods, which bring to sponge-like structures with interconnected pores (8). As previously reported, the pores interconnection grade and the scaffold three dimensional morphology determine cellular growth and proliferation; therefore it is essential that scaffolds are able to maintain their initial morphology. Furthermore, the ability of the scaffold in allowing the diffusivity of oxygen and nutrients through its porous structure is of great importance. Indeed, cells in the scaffolds, before the new tissue is completely formed, cannot be reached from blood vessels and so it is essential that oxygen and nutrients can permeate

through the scaffold interconnected pores and that this ability is kept for all the required time (9). The aim of this work was to evaluate the influence of PEG addition to regenerated fibroin on the stability of fibroin scaffolds upon incubation in terms morphology, mechanical properties and diffusivity capacity of oxygen through the scaffold. For this reason, all tests were conducted on fibroin and composite scaffolds immediately after their production and over an incubation period of 4 weeks. Indeed, after a long period in the human body or in an incubator for cell culture, it is important to check that the scaffolds characteristics necessary to cells development, and therefore tissue regeneration, are well preserved.

3.2 MATERIALS AND METHODS

3.2.1 Materials

Cocoons of B. mori silkworm silk were kindly supplied by ISMAC-CNR (Biella, Italy).

Calcium chloride dehydrate was purchased from Carlo Erba Reagenti (I).

Sodium metabisulfite was provided by Farmalabor (I).

Poly (ethylene glycol) 600 (PEG600; hydroxyl value = 170–208 mg KOH/g; Mw = 540–660 Da) was provided by Polichimica (I).

All solvents and reagents were of analytical grade, unless specified.

3.2.2 Preparation of regenerated B. mori silk fibroin solutions

Regenerated fibroin solutions (SF) were obtained by degumming raw B. mori silk and dissolving an appropriate amount of the degummed silk fibres in 100 mL $CaCl_2$ hydroalcoholic solution ($CaCl_2/H_2O/EtOH$, mole ratio 1:8:2) at 70 °C for 2 hours and shaken at 200 rpm in a thermostated bath. The regenerated fibroin was dialyzed in a cellulose tube (MWCO 12,000 Da, Sigma-Aldrich, I) against distilled water for 2 days at room temperature to eliminate salts and ethanol present in the solution. The final solution was filtered with a metallic strainer and, then, centrifuged for 20 min at 5000 rpm to eliminate the precipitated

fibroin. The final fibroin solution concentration was about 3.2% (w/w), determined by weighting the remaining solid after drying comparing the weight of the fibroin solution before freeze-drying (Ws) with the final weight of the scaffold after the freeze-drying process (Wf).

$$RF=Wf/Ws \cdot 100$$

3.2.3 Blends preparation and scaffold fabrication by freeze-drying

Before the freeze drying process fibroin blends were prepared just mixing the regenerated fibroin solution with PEG600 in the ratios of 95/5 % w/w and 90/10 % w/w following the geometric dilutions technique. Glass vials, filled with 3 mL pure fibroin solution or with the SF/PEG600 blends, were placed on a pre-cooled shelf at -20 °C inside the ice condenser chamber of an Alpha 1-4 LSC Christ (G) freeze-dryer and when the complete solidification was evident, samples were maintained at -20 °C for at least 8 hours. Once frozen, all samples were dried under the following condition: main drying: The shelf temperature was ramped from -20 °C to 25 °C in 5 hours; afterwards it was kept constant for 8 h. The chamber pressure was set at 2.380 mBar; final drying: the chamber pressure was set at 0.001 mBar. The shelf temperature was kept at 35 °C for 4 hours.

The final SF concentration of about 3 % (w/w), was determined on the basis of the dry weight of scaffolds. Upon completion of the drying, the scaffolds stoppered under vacuum and stored at room temperature until use.

3.2.4 Scaffold sterilization with steam under pressure method

The scaffolds were sterilized with the steam under pressure method in an autoclave (Tuttnauer 2540ML, N) using the conditions that are reported in the Official Italian Pharmacopeia XII edition (121°C, 1,2 bar, 15 min).

3.2.5 Molecular conformation

FTIR measurements were performed using a SpectrumTMOne spectrophotometer (Perkin-Elmer, USA), by placing the samples on a diamond crystal mounted in ATR cell (Perkin-Elmer, USA). The spectra recorded at 2 cm^{-1} resolution and 32 scans were collected over the wavenumber region 4000–650 cm^{-1}. The analyses were performed on raw polymers and scaffolds before and after sterilization. Fourier self-deconvolution (FSD) of the overlapping amide I band components (1585-1700 cm^{-1}) was made possible by using Peakfit 4.12 software (Galactic Industries Corporation, New Hampshire, USA). Spectra were baseline corrected, smoothed with a nine-point Savitsky−Golay function (10). The amide I bands were resolved by the second-order derivative with respect to the wavelength. Deconvolution was performed using Gaussian line shape with an amplitude threshold of 3%. A nonlinear least-square method was finally used to take the reconstituted curve as close as possible to the original deconvoluted spectra. The fitting results were further evaluated by examining the residual from the differences between the fitted curve and the original curve.

DSC data were recorded by using a DSC 2010 TA (TA Instruments, USA). The samples were sealed in aluminium pans and heated in inert atmosphere (70 mL/min N2) at 20 K/min from 30 to 350 ◦C. The reference was an empty pan. The equipment was calibrated with an indium sample. All measurements were performed in duplicate.

X-ray diffraction spectra of scaffolds before and sterilization were collected by using a Rigaku DMAX powder diffractometer (Rigaku, J) with Cu-Kα radiation and a monochromator on the diffracted beam.

3.2.6 Swelling properties

The swelling ratio of the scaffold and the water content in the scaffold were calculated as follows:

$$\text{Swelling ratio} = (Ws - Wd)/Wd \qquad \text{eq.1}$$

$$\text{water uptake (\%)} = [(Ws - Wd)/Ws]*100 \qquad \text{eq.2}$$

Porous fibroin and composite scaffolds were immersed in distilled water at room temperature for 24 h. Then, the wet weight of the sample (Ws) was determined after removing excess water. Scaffolds were dried in an oven at 60°C for 24 h and the dry weight of samples (Wd) was determined. All results are averages of triplicate measurements (±SD).

3.2.7 Morphology

The morphology of scaffolds was analyzed by SEM (JSM-T 800-JEOL, Italy). The specimens were sputtered with an Au/Pd coating in an argon atmosphere then they were analyzed with a spot of 3.5, 10 kV acceleration voltages and a WD of 10.

The scaffold morphology was evaluated also after 4 weeks scaffold incubation in a Dulbecco Modified Eagle Medium (DMEM). After the end of the incubation period the scaffolds were rinsed in a pH 7.4 PBS and fractured after immersion in liquid nitrogen. The scaffold sample were then observed without coating with gold at 10 kV acceleration voltages at vacuum pressure levels in the range of 0.9-4.0 Torr and at a constant temperature of 5°C.

Both the scaffold surface and its internal structure were observed. The mean pore size of the scaffolds was determined by analysis of the SEM and E-SEM images of the scaffold cross-section by importing data to Image-J software. Ten apparent pores per frame (30 frames per sample) were measured for each type of scaffold.

The open porosity (π) of SF scaffolds was calculated by a solvent displacement method (11). The scaffolds were submerged in a known volume (V1) of hexane that is not a solvent for SF and a series of brief evacuation–repressurization cycles was conducted to force the liquid into the pores of the scaffold. After these cycles, the volume of the liquid and liquid-impregnated scaffold was determined (V2). When the liquid-impregnated scaffold was removed, the

remaining liquid volume was measured (V3). The open porosity is calculated according to equation 3:

$$\pi = (V1-V3)/(V2-V3) \qquad \text{eq.3}$$

3.2.8 Mechanical properties

Fibroin and composite scaffolds were incubated in pH 7.4 PBS and stirred in a horizontal shaker incubator (50 strokes/min) at 37±1 °C (Julabo SW22, Germany). At specified time points (i.e. 7, 14, 21 and 28 days), specimen were removed and gently wiped. The mechanical properties of scaffolds were measured by a software controlled dynamometer (AG/MC, Acquati, Italy) equipped with a stainless steel probe (diameter: 4 mm) connected to a 5 daN force cell. Three samples of each scaffold were tested. The scaffolds were compressed at a cross head speed of 3mm/min. Load and displacement was noted.

3.2.9 Oxygen diffusivity

Before performing the test, the scaffolds were cut in 1 mm sections with a vibratome , and incubated in 3 ml DMEM + 10% antibiotic antimycotic solution 100x (10000 units penicillin, 10 mg streptomycin and 25 µg amphotericin B per ml) + 10% FBS for a total time of 4 weeks performing the experiments every week from day 0 to week 4. Every time the experiment was performed, the membranes were rinsed in pH 7,4 PBS and then fixed in the instrument on the

platinum electrode at the base of the cell in which 5 ml pH 7,4 PBS was put and the reference and the control electrodes are immersed. The technique is i-t Amperometry, with an initial E of -0,65 V. The sensitivity of the instrument is $1e^{-6}$ and the sampling interval is 0,5 sec.

For the evaluation of the oxygen diffusivity through the scaffold 5 ml of pH 7.4 PBS were put into the cell and nitrogen was made flow into the cell to remove the oxygen until the current was stable and the signal reached a steady line; at this point 2,5 ml of the PBS were removed and 2,5 ml of an oxygenated PBS were added and the signal was registered.

The registered signal is given from the time passed from the first moment in which the current is stable until the time the current is stable again after the variation due to the passage of the evaluated substance.

The diffusivity was determined in terms of diffusion coefficient (12), calculated using the equation 4:

$$D = L^2/t_{0.5}*0.1388 \qquad \text{eq.4}$$

where:

D = diffusion coefficient

L = thickness of the scaffold layer

$t_{0.5}$ = half of the diffusion time

3.3 RESULTS AND DISCUSSION

3.3.1 Scaffold structural and morphological properties

The scaffold porosity measurement, evaluated with the hexane displacement method, allowed determining quantitatively the porous structure of the different types of scaffolds. The results, reported in **Table 1**, demonstrate how the presence of PEG600 was able to significantly increase the scaffold porosity.

Table 1. Porosity of pure fibroin and composite scaffolds

Scaffold composition	Scaffold porosity (% v/v)
SF	78.4 ± 7.1
SF/PEG600 95/5 % w/w	93.9 ± 2.5
SF/PEG600 90/10 % w/w	93.8 ± 2.4

In order to evaluate the complex morphology of the scaffolds that couldn't be determined by a simple porosity measurement, the samples were observed with an electronic microscope to verify the size of the pores and their interconnectivity. First of all, the SEM pictures were registered on the untreated scaffolds immediately after lyophilization and the sterilization treatment, in order to confirm that the process didn't have any damaging effect on the

scaffold architecture. All the scaffolds presented a satisfactory internal organization, with a pore size ranging from 50 to 100 µm, appropriate for the cells to penetrate and live in. A decrease in the total scaffold porosity after sterilization didn't take place, so we can affirm that the steam under pressure treatment doesn't affect the scaffold structure, since porosity, pore size and pore interconnection of the scaffold are preserved, as the SEM pictures demonstrated. Considering that this event didn't affect the amount of the scaffold total porosity and that this value was fully satisfactory, this factor can be considered of minor importance. **Figure 1** shows an internal section of the scaffolds, reporting that the effects of the sterilization were not significant. The sterilized scaffolds resulted as responding to the tissue engineering requirements and are suitable for cell culture and tissue regeneration.

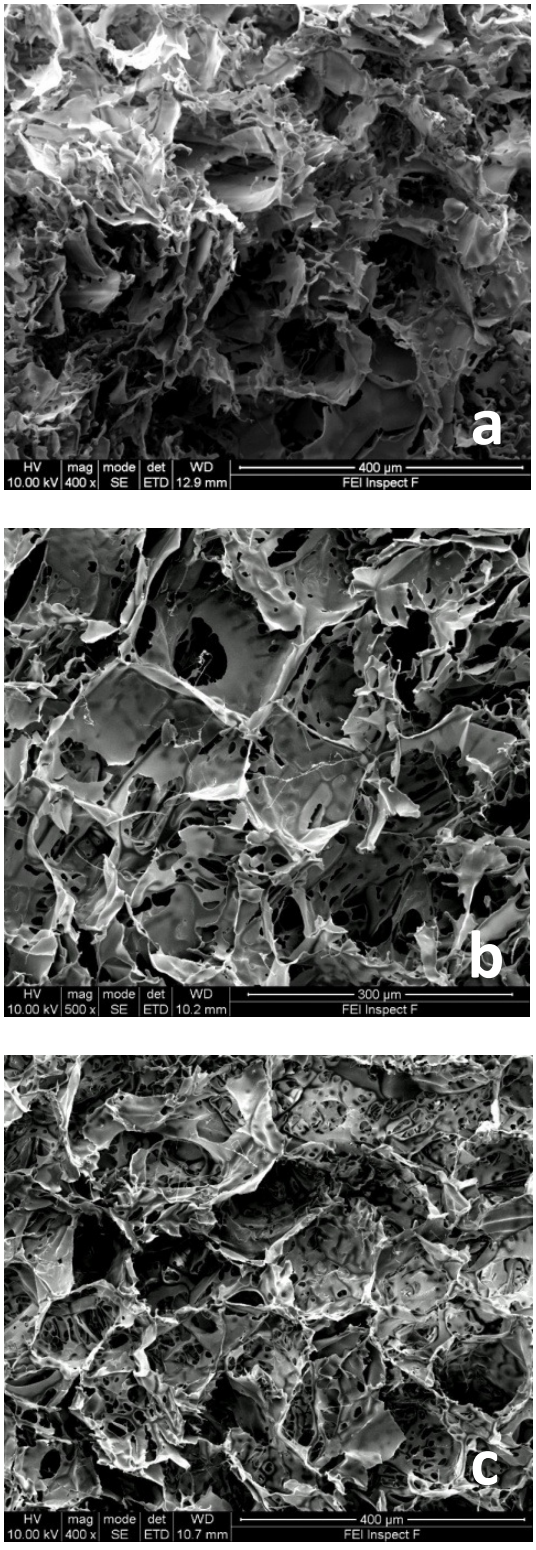

Figure 1. SEM pictures after autoclave treatment of scaffolds made of a) fibroin, b) fibroin/PEG600 95/5 % w/w c) fibroin/PEG600 90/10 % w/w

SEM and E-SEM pictures were taken also after the incubation of the three types of scaffolds in growth medium (Dulbecco's Modified Eagle Medium: DMEM) for 4 weeks, to check the resilience of the scaffolds in a physiologic environment in terms of morphology and structural architecture. The SEM pictures after incubation were taken after a scaffolds drying treatment in an oven at 37°C, in order to process them with the gold coating necessary to visualize the scaffolds in the electronic microscope. The analysis of the pictures showed a significant difference among the pure fibroin scaffolds and the composite ones (**Figure 2 a-c**). The fibroin/PEG scaffolds, indeed, showed maintenance of the porous structure in size and interconnectivity of the pores, whilst the fibroin scaffold architecture was deeply affected by the incubation/drying process, with a flattering of the pores probably due to a structure contraction and collapse that diminished the pore size and eliminated the interconnection between the pores.

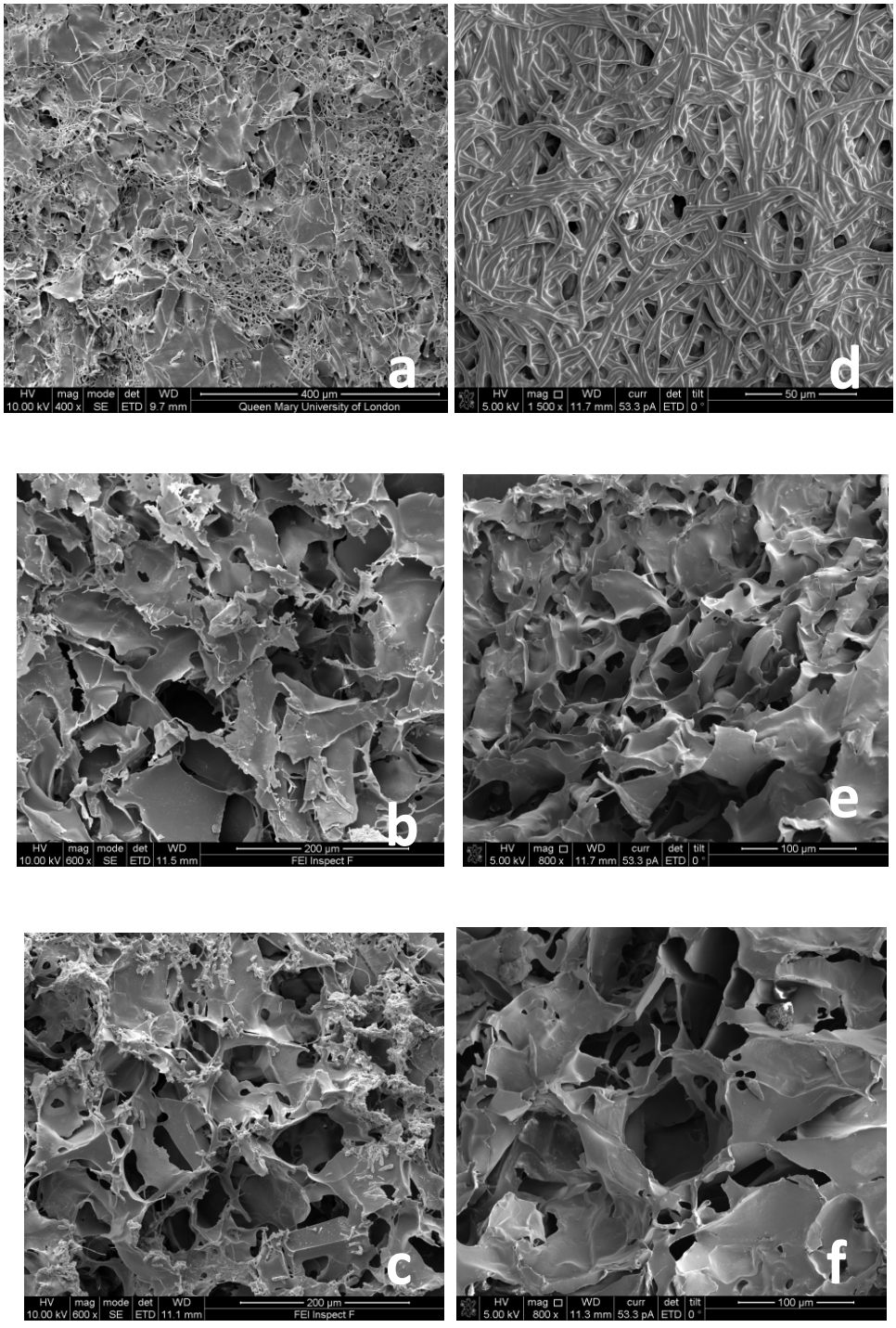

Figure 2. Scaffold morphology after 4 weeks of incubation: SEM pictures of scaffolds made of a) fibroin, b) fibroin/PEG600 95/5 % w/w c) fibroin/PEG600 90/10 % w/w and cryo E-SEM pictures of scaffolds made of d) fibroin, e) fibroin/PEG600 95/5 % w/w f) fibroin/PEG600 90/10 % w/w.

In order to check if the drying process after incubation and not the incubation procedure was the actual responsible for the fibroin scaffolds structural changing, an E-SEM was carried out on the samples. This kind of microscope imaging is really similar to the SEM one but with this version it is possible not to coat the samples or treat them in any way before the analysis, so that it is possible to look at them in their original state. A kind of E-SEM is the cryo SEM in which the samples are immersed in liquid nitrogen before the microscopic analysis so that they can preserve the shape they have without being influenced by the high vacuum present in the microscope chamber. In this way we could avoid the drying phase on the scaffolds, just rinsing them from the growth medium and freezing them in order to keep the features of the porous structure unaltered as they were in the physiologic environment at the end of the 4 weeks incubation (**Figure 2 d-f**). The results that emerged from this analysis were similar to the ones reported with the normal SEM: the pure fibroin scaffold structure was altered, whilst the composite scaffolds architecture was still the same as before the incubation period. This result signifies that the incubation procedure was the actual reason for the pure fibroin structural modification, not caused just by the stress of the water evaporation during the drying phase. The explanation for this difference between the fibroin scaffolds and the fibroin/PEG ones can be that the addition of the hydrophilic polymer to the protein was able to stabilize the net of the scaffolds architecture in a way that allow the construct to remain stable whilst immersed in an aqueous medium for a relative long time.

The ATR-FTIR analysis was carried on in order to evaluate the percentage of fibroin in the β-sheet conformation in the scaffolds realized with pure fibroin and composite scaffolds after the sterilization treatment. Considering the positive results obtained with 2D scaffolds realized by casting with the addition of 5-10% of PEG600, a quantitative evaluation was made on the composite 3D scaffolds realized by lyophilization to check if the addition of PEG could be able in allowing the achievement of higher percentages of β-sheet fibroin in the scaffolds. A qualitative analysis of the ATR-FTIR spectra realized on the sterilized scaffolds revealed that fibroin was prevalently in the β-sheet form. As shown in **Figure 3** the amide I and III band were detected at about 1620 and 1225 cm^{-1} respectively and both presented a shoulder on the left of the band. These wavelength values and the presence of the shoulders on the amide bands is diagnostic, since they're typical of fibroin in the β-sheet conformation (13).

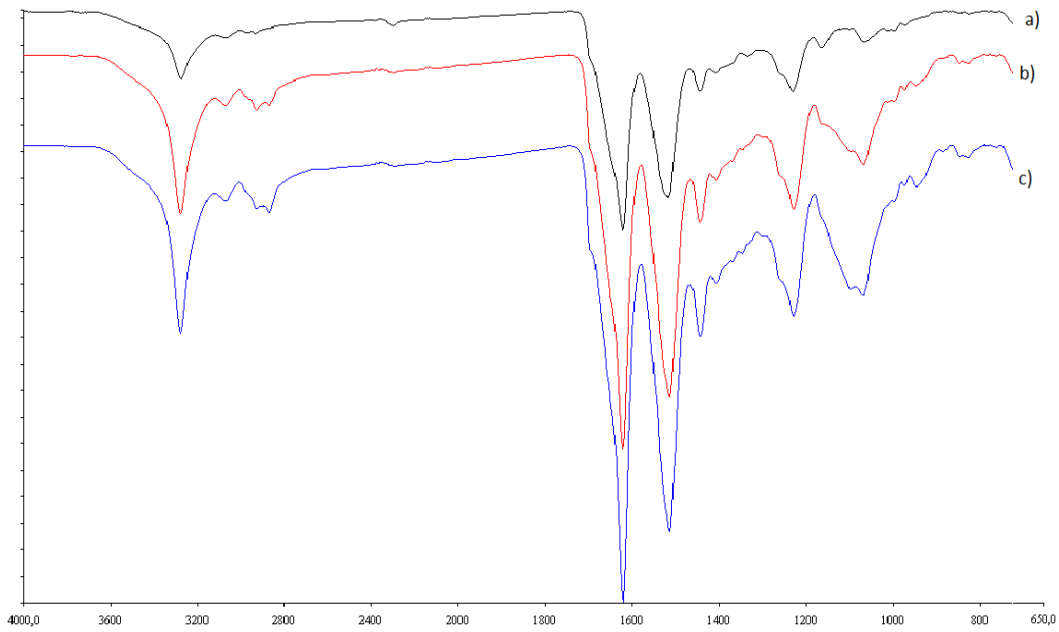

Figure 3. ATR-FTIR spectra of fibroin scaffolds made of a) pure fibroin, b) fibroin/PEG600 95/5 % w/w, c) fibroin/PEG600 90/10 % w/w scaffolds

A deeper insight into the fibroin conformation was performed deconvoluting the spectra of the amide I bands. **Figure 4** shows the typical deconvoluted amide I band which presented twelve peaks attributed to the different conformation of the protein, namely random coil that is considered as amorphous, α-helix and β-turn that are considered semi-crystalline structures, β-sheet that is the crystalline form and the side chains (14). As exemplified in **Figure 5** the addition of PEG600 slightly increased the β-sheet fibroin percentage in the scaffold. This slight increase, which appeared in contrast with data reported in Chapter 1, was justified considering that the selected sterilization procedure improved the transition of fibroin from a prevalent random coil/α-helix conformation to the most stable β-sheet form.

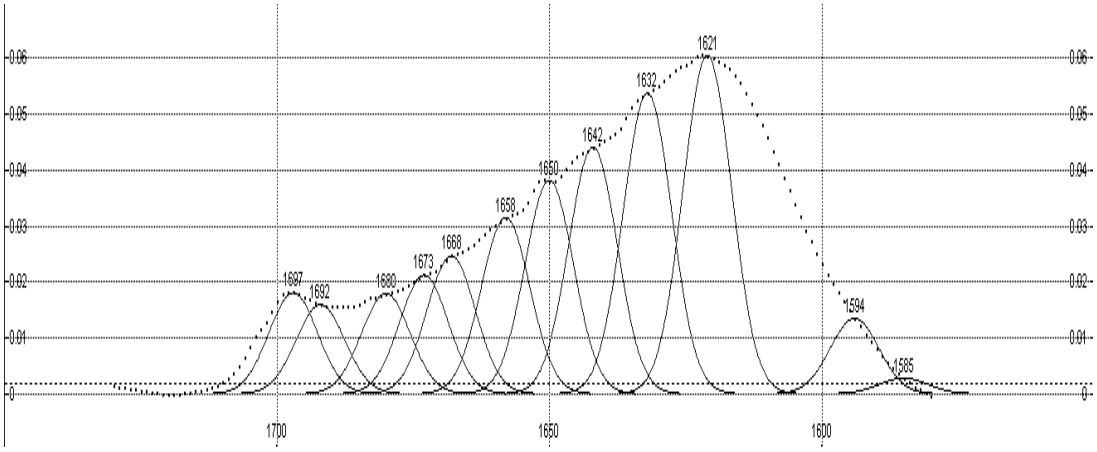

Figure 4. Amide I deconvoluted band of a β-sheet fibroin sample.

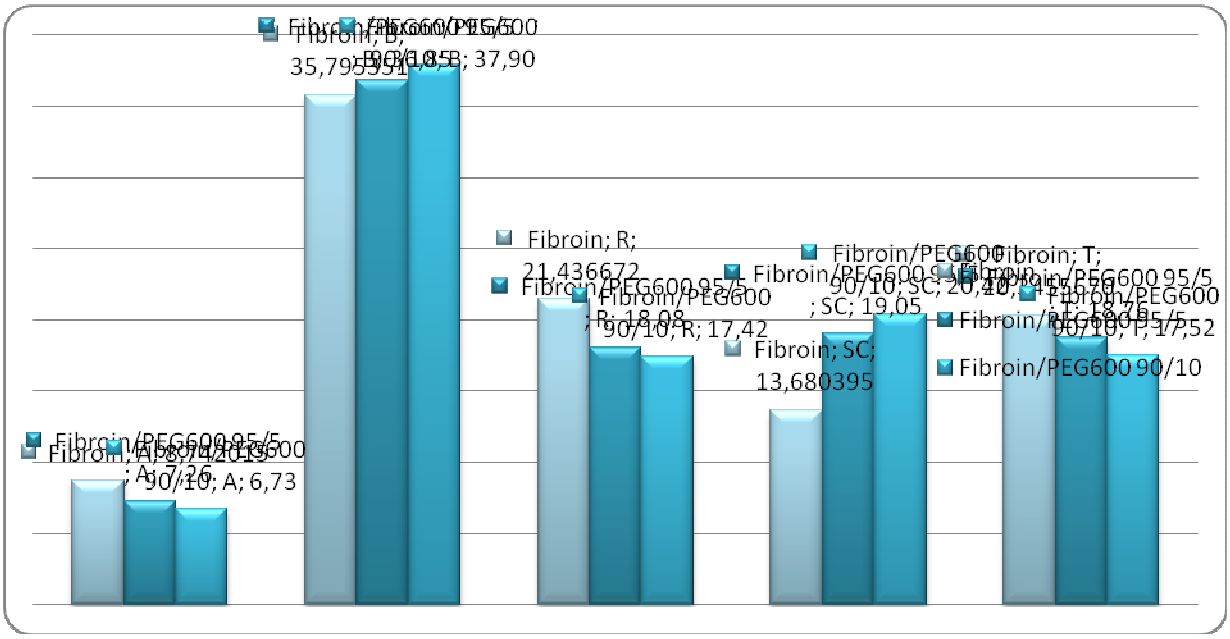

Figure 5. Comparison between the contributes of the different fractions on the total area of the absorbance amide I band of fibroin in scaffolds made of fibroin, fibroin+PEG600 95/5 % w/w, fibroin+PEG600 90/10 % w/w. A = α-helix, B = β-sheet, R = Random coil, SC = Side Chains, T = β-turn

The DSC analysis basically confirmed the results showed by the ATR-FTIR spectra analysis. The fibroin and the composite scaffolds were prevalently in the β-sheet conformation after the steam under pressure treatment, and the amount of fibroin in the crystalline form slightly grew with the addition of PEG. As shown in **Figure 6** the thermograms of all the scaffolds after sterilization appeared as the typical layouts of a crystalline protein, confirming the ordered spatial organization of fibroin in the scaffolds after sterilization, but not evidencing great difference between the results obtained on pure fibroin and composite scaffolds that were extrapolated, instead, by calculating the areas of the crystalline fibroin melting peaks. The pattern of all the scaffolds after sterilization didn't show the glass transition temperature at 179 ◦C, typical of the random coil conformation nor the exothermic peak at 218 ◦C (23 J/g) attributed to the transition from random coil to β-sheet structure. This result demonstrated the presence of small amounts of random coil/α-helix fibroin and the prevalence of the β-sheet form. An endothermic event related to water evaporation was registered at about 100 ◦C. Thermal decomposition of the material was registered at 299 ◦C, a peak that is attributed the crystalline material.

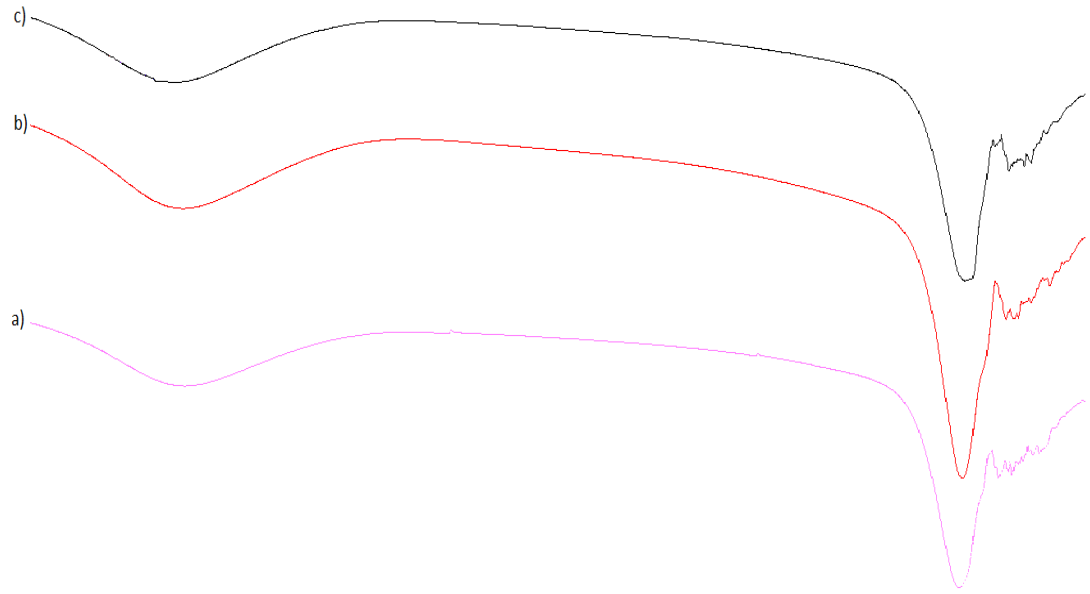

Figure 6. DSC data of sterilized scaffolds made of a) fibroin b) fibroin+PEG600 95/5 % w/w c) fibroin+PEG600 90/10 % w/w

The effect of incubation on the fibroin conformation was studied by x-ray diffraction. The x-ray patterns were registered on the pure fibroin and the composite scaffolds after sterilization, both before and after the incubation period of 4 weeks in DMEM. This analysis was carried out to confirm the fibroin crystalline conformation in the scaffolds put through the sterilization treatment and to check any possible changing in the fibroin conformation after a long period immersed in physiologic environment. The results, as reported in **Figure 5** showed the differences among the different kind of scaffolds as they appeared before and after an incubation period of one month. Looking at the patterns registered on the scaffolds before incubation, it is evident that all the scaffolds presented the same behavior at the x-ray diffraction, showing the same fibroin

conformation for the scaffolds made of pure fibroin and the ones made from fibroin/PEG mixtures. In **Figure 7** it is possible to recognize, for all the three patterns, two main peaks at about 20-21° and 25-26°. The peak at 20-21° is attributable to the β-sheet crystalline structure of fibroin, which is shown in the silk fabric XRD spectrum (15). This result indicates that the β-sheet crystalline structure exists in the scaffolds, but the comparison of the peak strengths with the reference of the silk fabric shows that the amount of the crystalline structure is smaller in the scaffolds. As a matter of fact, the peak at 25-26°, instead, is attributable to the α-helix structure (15), which also exists in the fibroin scaffolds. For all the scaffolds analyzed after the incubation in growth medium for one month, it is possible to evidence a substantial decrease in the registered signal power, demonstrating a global decrease in the crystalline fibroin content for all the tested scaffolds. Looking at the graphs reported in **Figure 7** it is evident that the graphs of the scaffolds realized form the fibroin/PEG blends (**Figure 7**) are completely superimposable, presenting the same x-ray patterns, with the maintenance of two distinct peaks for the β-sheet and the α-helix conformations as at the beginning of the incubation period. The x-ray pattern of the pure fibroin scaffold after the incubation (**Figure 7**), instead, showed a significant decrease in the peak at 20-21° typical of the β-sheet form, demonstrating a variation of the fibroin conformation during its long permanence in the physiologic environment. This result evidenced the PEG capacity in stabilizing the fibroin structure in terms of molecular conformation when the scaffolds are immersed for a long period in an aqueous system.

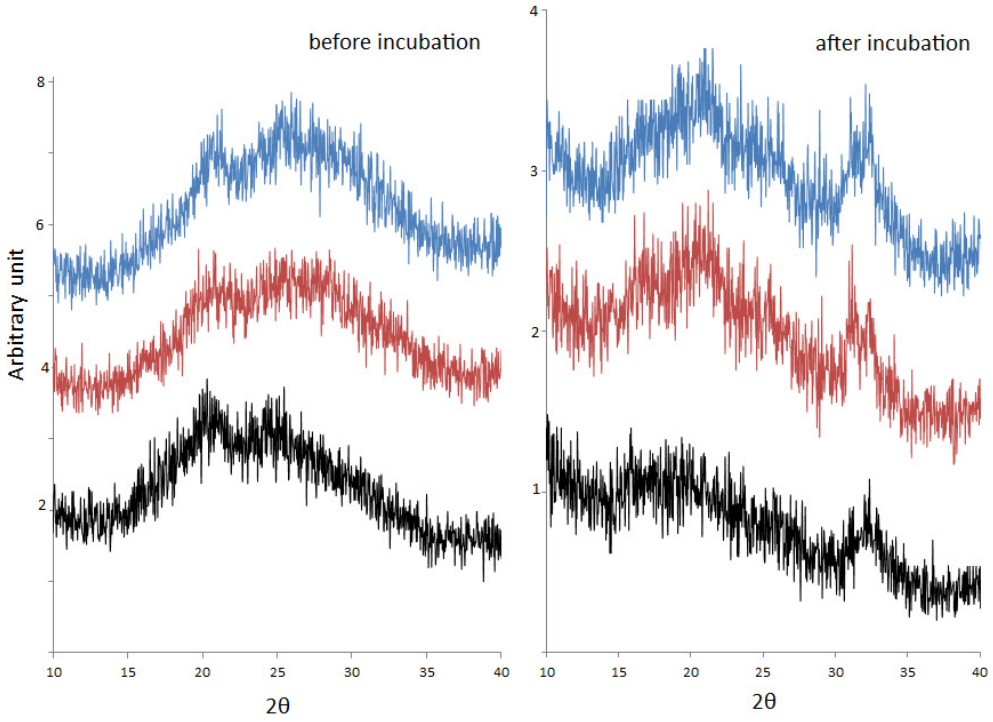

Figure 7. X-ray patterns of sterilized scaffolds made of fibroin (black line), fibroin/PEG600 95/5 % w/w (red line) and fibroin/PEG600 90/10 % w/w (blue line) before and after 4 weeks incubation in DMEM.

The water binding ability of the scaffold was also evaluated, since it is an important feature to consider in relation to biomaterial properties for tissue engineering. Three samples of each formulation were used to measure the swelling ratio and water uptake after the sterilization treatment, to allow the fibroin conformational change into the β-sheet water stable form. During 24 h, the average value of swelling ratio and water uptake were not significantly different for all the tested formulations, showing that no difference in water affinity is caused by the PEG addition to the fibroin scaffolds. Indeed, the data reported in **Table 2** show just slight differences between the swelling ratio values for the pure fibroin and composite scaffolds, with a mean value around 26 and a

standard deviation that make the results not statistically different one from the other. These results, together with a water uptake value of about 96% for all the considered samples, indicate excellent hydrophilicity both for the pure fibroin and the composite scaffolds, confirming their suitability for the implantation in the human body.

Table 2. Scaffold swelling ratio and water uptake after the sterilization procedure

Scaffold composition	**Swelling ratio**	**Water uptake (%)**
SF	26.5 ± 3.04	96.33 ± 0.43
SF/PEG600 95/5 % w/w	25 ± 1.34	96.14 ± 0.2
SF/PEG600 90/10 % w/w	28 ± 2.7	96.55 ± 0.33

3.3.2 Mechanical testing: compression resistance by texture analysis

All samples of pure fibroin and composite scaffolds exhibited ductile and sponge-like behavior, both in the dry state at time zero of the incubation period and in the wet state during their immersion in physiologic environment (pH 7.4 PBS) for a period of 3 weeks. An elastic region was observed at the initial stage of strain followed by a peak stress. The peak stress was followed by a nearly constant flow stress region. Finally, a densification region where the flow stress increases steeply was observed in all samples. The maximum load registered for the pure

fibroin structures was around 0.25 N for the dry scaffold, but this value rapidly decreased during the following weeks of incubation (**Figure 8**).

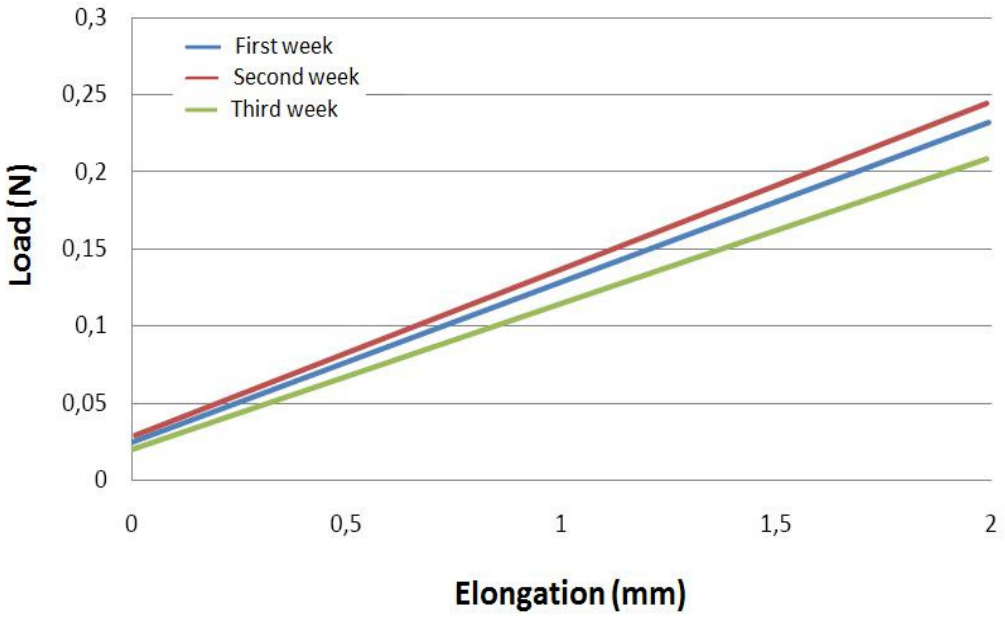

Figure 8. Mechanical resistance profile of a pure fibroin scaffold registered at time 0 and after 1, 2 and 3 weeks of incubation in pH 7.4 PBS at 37 °C.

For the scaffolds realized with fibroin and PEG600 in the ratio 95/5 % w/w and 90/10 % w/w the initial maximum load value was significantly lower, around 0.1 N and 0.15 N respectively, but it was well preserved during all the incubation period (**Figure 9**). This suggested that PEG600 has a plasticizing effect on the fibroin chains, making the scaffolds more elastic and less stiff. The maintenance of the same compression resistance in the physiologic environment demonstrated a structural integrity of the composite scaffolds. This was already

demonstrated by the analysis of the SEM pictures taken after the scaffolds 4 weeks incubation in physiologic environment. The fibroin/PEG scaffolds showed maintenance of the porous structure in size and interconnectivity of the pores, whilst the fibroin scaffold architecture was deeply affected by the incubation process, with a flattering of the pores due to a structure contraction and collapse that diminished the pore size and eliminated the interconnection between the pores. This different behavior was easily explained with the fact that the interconnected pores structures of the composite scaffolds are more stable during the time without any variation of the scaffold internal morphology, because PEG600 is able to stabilize the fibroin chains. In addition, it has been reported that more uniform pore distributions in scaffolds improves mechanical properties of the polymer matrices. Stress applied to porous materials is concentrated at pore interfaces, and if the pore distribution is not uniform, as in the case of pure fibroin scaffold respect to the composite one, polymer matrices typically deform at lower stress.

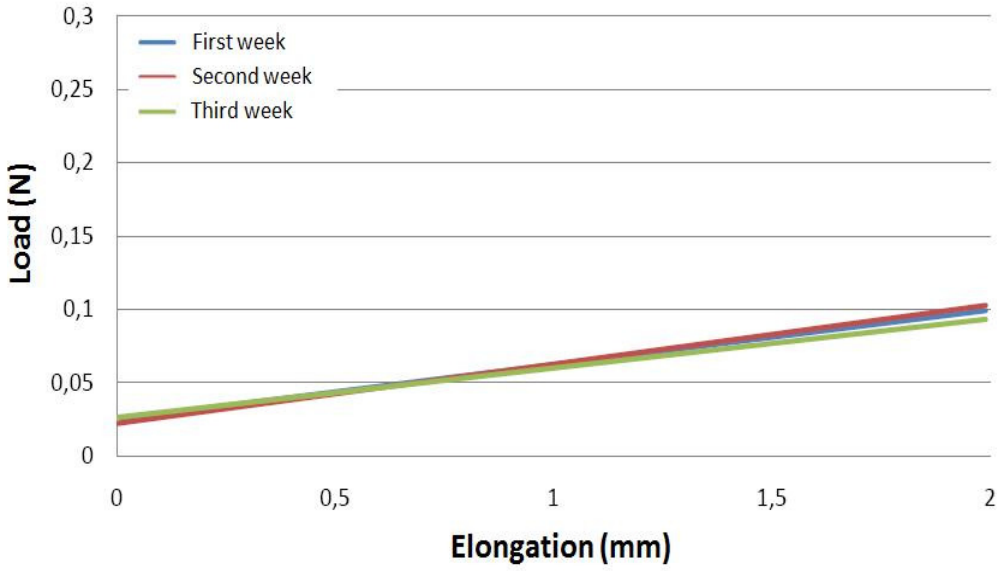

Figure 9. Mechanical resistance profile of a fibroin/PEG600 95/5 % w/w scaffold registered at time 0 and after a 1, 2 and 3 weeks of incubation in pH 7.4 PBS at 37°C.

3.3.3 Diffusivity through the scaffold

Considering that in the field of tissue engineering a scaffold should serve as an incubator for cells, not just a supportive function is required from it, but also an ability to keep the cells alive during their differentiation and proliferation phase, in order to allow the regrowth of the tissue contemporary to the scaffold degradation. In order to keep the cells viable during this period of time, it is necessary to assure them the right amount of oxygen and nutrients, and since they can't be reached from blood vessels the scaffold must allow the diffusion of these molecules through its structure composed of interconnected pores (16). A test was then conducted to verify the diffusivity of oxygen through the scaffolds during an incubation period of 4 weeks. Three samples of each formulation were

used for every measurement. In **Figure 10** an example of the registered graphs is reported for the oxygen diffusion test.

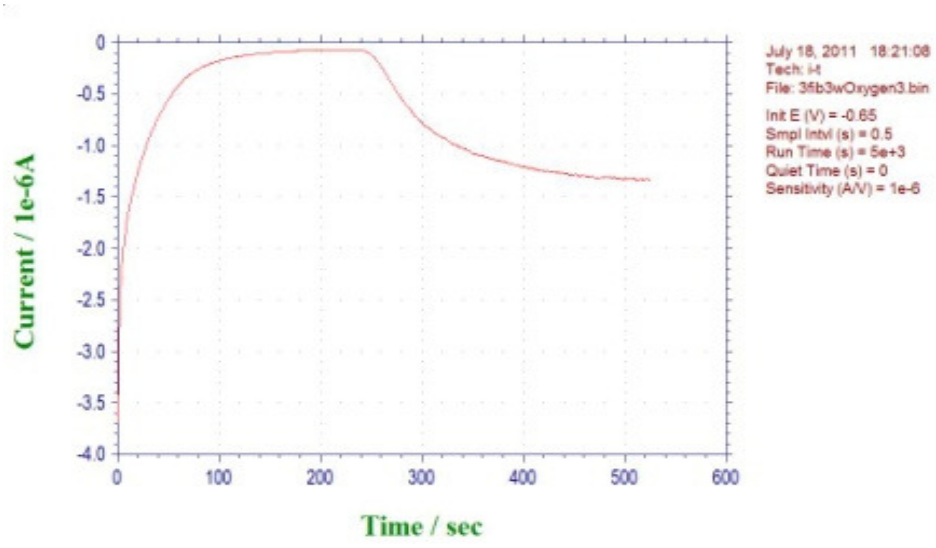

Figure 10. Graphs obtained with an amperometric method and representative of the oxygen diffusivity through a fibroin scaffold

Analyzing the graphs it is possible to calculate the time necessary to pass from the initial steady current to the final steady current that is restabilized after the current increase due to the molecule diffused through the scaffold and detected by the working electrode. This value is defined as the diffusion time and it is used in the following equation to determine the diffusion coefficient of the molecule through the scaffold and to have an estimation of the scaffold diffusivity capacity respect to that particular molecule.

$$D = L^2/t_{0.5}*0.1388$$

D = diffusion coefficient

L = thickness of the scaffold layer

$t_{0.5}$ = half of the diffusion time

Comparing the diffusion coefficients of every analyzed substance during the 4 weeks of incubation, it was possible for every kind of scaffold to construct a graph representative of the diffusivity trend during the time. It is possible to understand from the analysis of the data reported in **Figure 11** that significant variations can be seen among the different kind of scaffolds in terms of diffusivity of oxygen, since the diffusivity coefficients are significantly different during all the incubation time. As a matter of fact, the behavior of the pure fibroin and composite scaffolds is completely opposite: the oxygen diffusivity through the pure fibroin scaffold is constantly diminishing during the incubation time, whilst it is rather constant for the fibroin/PEG600 scaffolds, demonstrating also in this case that PEG600 is able to maintain the scaffold features in a physiologic environment during a prolonged period of time.

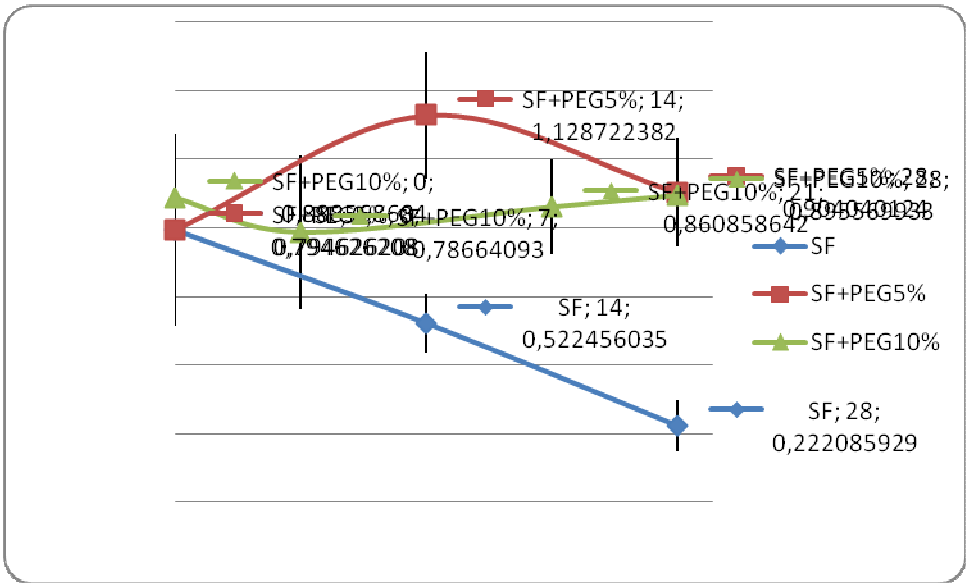

Figure 11. Diffusion coefficient of oxygen through pure fibroin and composite scaffolds during a 4 weeks incubation period.

PEG is evidently able to maintain the scaffold structure, as previously reported, due to a stabilizing effect on the fibroin chains that allows the scaffold to keep its diffusivity properties also when it is incubated in a physiologic environment for a 1 month period. The pure fibroin scaffold, instead, after one month in growth medium, suffered from morphological variations that decreased its ability in oxygen permeation respect to the first day of incubation.

3.4 CONCLUSIONS

Porous scaffolds made of pure fibroin and fibroin/PEG600 were prepared directly from silk fibroin aqueous solutions by freeze-drying. The formation of these water stable scaffolds included a structural transition of fibroin from random coil/α-helix to β-sheet conformation due to a sterilization procedure with steam under pressure. Functional and morphological properties of the scaffolds were successfully controlled by the addition of PEG600. All the scaffolds presented satisfactory features in terms of fibroin conformation, internal architecture and water affinity. The porosity and pore size after the freeze-drying process are acceptable for every kind of scaffold but the porosity and pore interconnection resulted optimal when PEG600 was added. After an incubation period of 4 weeks, the advantages of the PEG addition to the fibroin solution for the preparation of composite scaffolds were even more evident. First of all the presence of PEG conferred to the scaffolds a great stability in terms of morphology and internal organization, which was well preserved during a prolonged period in the physiologic environment. Consequently, the composite scaffolds presented also good mechanical properties that were well maintained during all the incubation period. Indeed, even if the compression resistance values were initially lower for the composite scaffolds respect to the pure fibroin ones, the compression resistance ability was retained during all the considered time, whilst with the pure fibroin scaffolds a significant decrease was registered.

Finally, the PEG capacity of stabilizing the fibroin chains and hence the scaffold architecture, was reflected also in the ability of keeping the oxygen diffusivity through the scaffold constant for one month of immersion in physiologic conditions, assuring cells viability when the tissue isn't completely reformed yet. It is possible to say that scaffolds formed from regenerated fibroin and PEG result morphologically stable to incubation in growth medium for a period of time of one month, differently from the pure fibroin scaffolds. Therefore the composite scaffolds are more suitable for cell growth, hence for being suitable substitutes for damaged tissues. These results should be further analyzed and completed in terms of cell affinity in order to check the cells real viability in culture conditions on the composite scaffolds, but the data obtained are surely promising, evidencing the feasibility of a good platform centered on the use of fibroin and other polymers in order to modulate its properties.

REFERENCES

(1) Place et al, *Nature materials*, 2009, 8, 457-470

(2) Altman et al, *Biomaterials*, 2003, 24, 401-416

(3) Nazarov et al, *Biomacromolecules*, 2004, 5(3), 718-726

(4) Vepari & Kaplan, *Progress in polymer science*, 2007, 32, 991-1007

(5) Chen et al, *Acta chimica sinica*, 2003, 61(4), 625-629

(6) Cilurzo et al, *International journal of Pharmaceutics*, 2011, 414(1-2), 218-224

(7) Wang et al, *Chinese journal of polymer science*, 2003, 21(1), 87-91

(8) Kaplan et al, US 2010/0279112

(9) Place S. et al, *Chemical society reviews*, 2009, 38, 1139-1151

(10) Savitzky A. et al, *Analytical Chemistry*, 1964, 36, 1628−1639

(11) Karageorgiou V. & Kaplan D.L., Biomaterials, 2005, 26(27): 5474-5491

(12) Vadgama P., *Biomaterials*, 2006, 27, 4266-4268

(13) Boudet-Audet M. et al, *App. Spectrosc.*, 2008,62, 956-962

(14) Cilurzo F. et al, *International Journal of Pharmaceutics*, 2011, 414, 218-224

R&D ir deconv

(14) Marsh R.E. et al, *Biochemical and Biophysical Acta*, 1955, 16, 1-34 x-ray R&D

(15) Place E.S. et al, *Chemical society reviews*, 2008, 38, 1139-1151

General Conclusions

Composite materials were obtained by spray-drying or casting a 3% regenerated fibroin solution containing PEGs with molecular weights from 600 to 4000 in percentages ranging from 1 to 20. In the composite materials obtained by spray-drying the high water evaporation rate led to fibroin in the amorphous form. Films with suitable characteristics in terms of crystallinity and homogeneity were obtained by casting a 3% regenerated fibroin solutions containing PEGs with a molecular weight of 600 and 1000 in concentrations ranging from 5 to 20%.

Lyophilisation is the most commonly used method to prepare 3D scaffolds with porosity suitable for tissue engineering. Since the scaffolds are implantable systems they need to be sterilized. The sterilization with steam under pressure was selected because it is known (1) that high temperatures and water vapour are able to promote the transition from the protein amorphous form to the crystalline one. 3D scaffolds were obtained by freeze-drying a 3% regenerated fibroin solution. Their sterilization with steam under pressure induced the fibroin conversion to the β -sheet form and conferred the suitable mechanical properties.

An in-depth study was carried out on the scaffold formulation and lyophilisation cycle development. The considered process variables were the freezing temperature, the freezing time and the thermal treatment. The results evidenced that a freezing phase of at least 8 hours at -20°C was required to obtain stable structures and avoid the collapse of the scaffolds after the sterilization treatment. The thermal treatment, namely the freeze thawing,

allowed to increase the scaffold mechanical robustness. This feature can be ascribed to the different inner morphology since fibroin fibres were highly oriented perpendicular to the scaffold horizontal surface, instead of the sponge structures generally obtained using the conventional linear freezing process. Concerning the impact of the formulation variables, the fibroin concentrations in the regenerated solution deeply influenced the final properties of 3D scaffolds. Indeed, as the fibroin concentrations increased from 1 to 4%, a great improve in the mechanical robustness of scaffolds at the increase of the fibroin concentration was observed, along with a massive decrease in porosity and pore size. On the bases of these results, fibroin concentration was fixed at 3% w/w, since the features of scaffolds represented a suitable compromise between optimal porosity and satisfactory mechanical properties. Of particular interest was also the addition of small amounts of DMSO to the regenerated fibroin solution since the solvent improved the scaffold mechanical properties as well as the amount of β-sheet fraction of fibroin in the scaffold.

On the basis of the results obtained with 2D scaffolds, the mixture SF/PEG was also used to prepare 3D scaffolds. Even if PEG wasn't able to induce a fibroin conformational change, it allowed to increase porosity and pore size. The structural analysis on the scaffolds was conducted both before and after an incubation period of 4 weeks in growth medium. The main result was that the PEG addition allowed to maintain the scaffold architecture during all the incubation period, stabilizing the fibre organization inside the scaffold. The stabilization effect also involved the scaffold mechanical properties: the

composite material presented a lower compression resistance, but the value remained constant for all 4 incubation weeks, evidencing the polymer stabilizing effect on the scaffold structure.

The effect of the PEG addition on the oxygen diffusivity through the scaffolds was also extensively studied. The oxygen diffusivity through the pure fibroin scaffolds, constantly diminished during the overall incubation period, whilst this parameter remained rather constant for the fibroin/PEG600 scaffolds, demonstrating further on that PEG600 was able to maintain the scaffold architecture in a physiologic environment during a prolonged period of time.

In conclusion, the structural and mechanical properties of scaffolds along with their stability over time in physiological conditions can be improved designing composite materials made of fibroin and PEG as well as modulating the drying or freezing parameters during the production processes by casting and lyophilisation, respectively.